University of Windsor

Scholarship at UWindsor

7-7-2020

Optimal Protection Coordination of Active Distribution Networks Powered by Synchronverters

Saad Arshed Pola
University of Windsor

Optimal Protection Coordination of Active Distribution Networks Powered by Synchronverters

By

Saad Pola

A Thesis
Submitted to the Faculty of Graduate Studies
through the Department of Electrical and Computer Engineering
in Partial Fulfillment of the Requirements for
the Degree of Master of Applied Science
at the University of Windsor

Windsor, Ontario, Canada

2020

Optimal Protection Coordination of Active Distribution Networks Powered by Synchronverters

by

Saad Pola

APPROVED BY:

_____

A. Azab
Department of Mechanical, Automotive and Materials Engineering

_____

N. Kar
Department of Electrical and Computer Engineering

_____

M. Azzouz, Advisor
Department of Electrical and Computer Engineering

April 24, 2020

DECLARATION OF CO-AUTHORSHIP

I.   Co-Authorship

I hereby declare that this thesis incorporates materials that are results of joint research, which appear in Chapters 4, 5, and 6 were co-authored with Dr. Maher Azzouz, and he contributed to the overall coordination and improvements.

I am aware of the University of Windsor Senate Policy on Authorship, and I certify that I have properly acknowledged the contribution of other researcher(s) to my thesis and have obtained written permission from each of the co-author(s) to include the above materials in my thesis. I certify that, with the above qualification, this thesis, and the research to which it refers, is the product of my work under the supervision of Dr. M. Azzouz.

II.   General

I declare that, to the best of my knowledge, my thesis does not infringe upon anyone's copyright nor violate any proprietary rights and that any ideas, techniques, quotations, or any other material from the work of other people included in my thesis, published or otherwise, are fully acknowledged in accordance with the standard referencing practices. Furthermore, to the extent that I have included copyrighted material that surpasses the bounds of fair dealing within the meaning of the Canada Copyright Act, I certify that I have obtained written permission from the copyright owners to include such materials in my thesis.

I declare that this is a true copy of my thesis, including any final revisions, as approved by my thesis committee and the Graduate Studies office and that this thesis has not been submitted for a higher degree to any other University or Institution.

ABSTRACT

The integration of distributed generators (DGs) into distribution networks leads to the emergence of active distribution networks (ADNs). These networks have advantages, such as deferring the network upgrade, lower power losses, reduced power generation cost, and lower greenhouse gas emission, DGs are classified due to their interface with the network as inverter-interfaced or synchronous-interfaced.

However, DGs integration results in bidirectional power flow, higher fault current levels, deterioration of the protection coordination of the directional overcurrent relays (DOCRs) which are used in ADNs, reduced system stability due to the inverters' lack of damping. The stability can be enhanced by controlling the inverters to behave as synchronous generators, which are known as synchronverters.

In this thesis, a two-stage optimal protection coordination (OPC) scheme is proposed to guarantee reliable protection of ADNs while protecting synchronverters from overcurrent using virtual impedance fault current limiters (VI-FCLs). VI-FCLs provide a cost-effective way to protect synchronverters from overcurrent. The first stage integrates the fault current calculations of synchronverters in the fault analysis to find the parameters of VI-FCLs used to limit the synchronverter's fault current. In the second stage, the fault current calculations, along with the designed VI-FCLs from the first stage, are employed to determine the optimal relays' settings to minimize the total operating times for all the DOCR. It is found that fixed VI-FCLs can limit synchronverters' fault currents but may make the OPC problem infeasible to solve. Thus, an adaptive VI-FCL is proposed to ensure a feasible OPC under various fault conditions, i.e., locations and resistances.

DEDICATION

I dedicate my thesis work to my wife and my beautiful daughters. A special feeling of gratitude to my loving and supporting parents, whose words of encouragement and push for tenacity ring in my ears all the time. And to my siblings, who have never left my side.

ACKNOWLEDGMENTS

No words are adequate to express my sincere appreciation to my supervisor Dr. Maher Azzouz for taking me into this scientific field and providing me with valuable advice and guidance throughout my research. He's always kind and helpful. He's my inspiration through my academic and research carrier. I would also like to thank my committee members Dr. N. Kar and Dr. A. Azab; I have learned so much from them through their valuable comments and instructions.

TABLE OF CONTENTS

LIST OF TABLES

LIST OF FIGURES

CHAPTER 1

INTRODUCTION

1.1 Overview

Synchronverters are inverter-interfaced distributed generators (DGs) with a controller that mimics the behavior of synchronous generators (SGs). The synchronverter controller adds virtual inertia to avoid the unwanted attributes of traditional inverters, i.e., too fast and can't reject small disturbances [1]. However, a synchronverter may generate a current higher than its rated current when it is under a fault condition [2]. A possible solution to overcurrent conditions is by controlling the synchronverter as a current source. However, the directional overcurrent relays (DOCRs) may malfunction, thus, worsening the grid stability and complicating the short-circuit analysis. Virtual-impedance fault current limiters (VI-FCLs) are non-physical impedances added to the synchronverter's equivalent circuit by controlling its output current, as will be explained later. Equipping synchronverters with VI-FCLs can keep their voltage source model intact, and thus, enhancing the coordination of DOCRs. To ensure coordinated synchronverter protection, VI-FCLs should be considered in short-circuit current calculations and the optimal protection coordination (OPC). OPC is a process to determine the optimal settings of DOCRs that minimize the total operating time of all primary and backup relays [3]. In this thesis, it is proposed to equip synchronverters with VI-FCLs to ensure reliable and cost-effective protection of distribution networks without the need for communication or physical fault current limiters (i.e., extra hardware).

1.2 Objectives

The objective of this thesis is to develop a current limitation method for synchronverters in active distribution networks (ADNs). The developed current limitation method should keep the voltage source model of a synchronverter intact to be used in fault current calculations as a part of a proposed two-stage OPC scheme. The first stage of the proposed OPC scheme aims at sizing the VI-FCLs for short-circuit current calculations. The second stage determines the optimal relays settings that minimize the total operating time of primary and backup relays and maintain proper coordination to isolate the fault area.

The adopted synchronverter model with VI-FCLs is validated in twofold. First, the developed short circuit current calculations are compared with time-domain simulations. Second, the performance evaluation includes two systems, i.e., a grid-synchronverter system and a Canadian 9-bus distribution network. Further, the proposed OPC scheme that adopts fixed VI-FCLs is extended to accommodate adaptive VI-FCLs. The adaptive VI-FCLs enhance the performance of OPC and make it immune to different fault locations and resistances.

1.3 Thesis Organizing

This thesis comprises seven chapters that survey the literature, review the basics of the core topics, identify the problems under study, explain the proposed solution, and lastly, validate and evaluate the proposed solution. The thesis is organized as follows:

Chapter 2 reviews the literature on synchronverter modeling and control, OPC, and fault current limiter strategies. Shortcomings and gap analysis are illustrated in this chapter.

Chapter 3 explains the preliminaries to understand the operation principles of synchronverters and the generic formulation of the OPC program.

Chapter 4 states the problem of the high current generation from synchronverters during faults accompanied by time-domain simulations and demonstrates the necessity of the proposed two-stage OPC as opposed to the classic OPC program.

Chapter 5 demonstrates the design of the proposed VI-FCL controller along with time-domain simulations for synchronverters' current limitations and confirms the voltage source model of synchronverters with VI-FCLs. Further, this chapter formulates the proposed two-stage OPC scheme and explains each stage.

Chapter 6 shows simulation results that (i) validate the synchronverter voltage source model, (ii) evaluate the performance of the proposed two-stage OPC, and (iii) demonstrate the need for the adaptive VI-FCLs.

Lastly, Chapter 7 draws the thesis conclusions and suggests directions for future work.

CHAPTER 2

LITERATURE SURVEY

2.1 Introduction

The rate of distributed energy resources (DERs) integration is occurring at a higher pace due to the increasing concerns about carbon emissions caused by fossil-fuel power plants. DERs could contribute to reducing the prices of purchasing electricity and enhancing system reliability [4].

The integration of DERs, in the form of DGs, results in bidirectional power flow at the distribution level, and hence, the evolution of ADNs [5]. However, the integration of renewable-based DGs comes at a cost. In addition to their intermittent power nature, renewable-based DGs have no inertia, and therefore they could adversely impact the system stability [6].

2.2 Synchronverter Modeling and Control

To overcome the lack of damping caused by renewable-based DGs, it is imperative to equip the DG controller with a means to reject disturbances. To enhance the system damping, the concept of synchronverters emerged [1]. A synchronverter is an inverter with a novel control scheme that mimics the behavior of SGs. The synchronverter has all the good and bad attributes of an SG. Synchronverter parameters of a can be chosen to eliminate the magnetic saturation and eddy currents. The lost energy of an SG due to friction is not lost in a synchronverter; it is directed back to the inverter's DC bus.

The synchronverter operational characteristics are also applied to static synchronous compensator (STATCOM) to mimic synchronous condensers. The mathematical model of SG operates in the compensator mode is utilized without a phase-locked loop (PLL) [7]. Also, the synchronverter concept is applied to back-to-back converters used in high-power wind-based DGs [8]. The converters on both sides run as synchronverters. The outcome was to make wind-powered systems more friendly. The novel synchronverter algorithm proposed in [1] is updated to eliminate the need for a PLL unit [9]. It can automatically synchronize with the grid, track the grid frequency after reconnection, and it exhibits better dynamic performance with reduced complexity and less computational burden. This synchronverter is known as a self-synchronized synchronverter.

Synchronverters are modeled as a voltage source behind their interfacing filter impedance. Consequently, a synchronverter could suffer from high inrush currents during short-circuit faults, which can break down its power electronic switches [2]. Therefore, a fault current limiting strategy is required to limit its fault current.

2.3 Fault Current Limiters

Fault current limiters (FCLs) are series devices to hold short-circuit currents below the desired value. FCLs should have zero impedance during regular operation, have large impedance during fault events, and withstand the grid voltage. FCLs are also required to have a long lifetime, high reliability, and be fast-acting and recovering [10]. FCLs are available in different topologies and technologies, as categorized in Figure 2.1 [11].
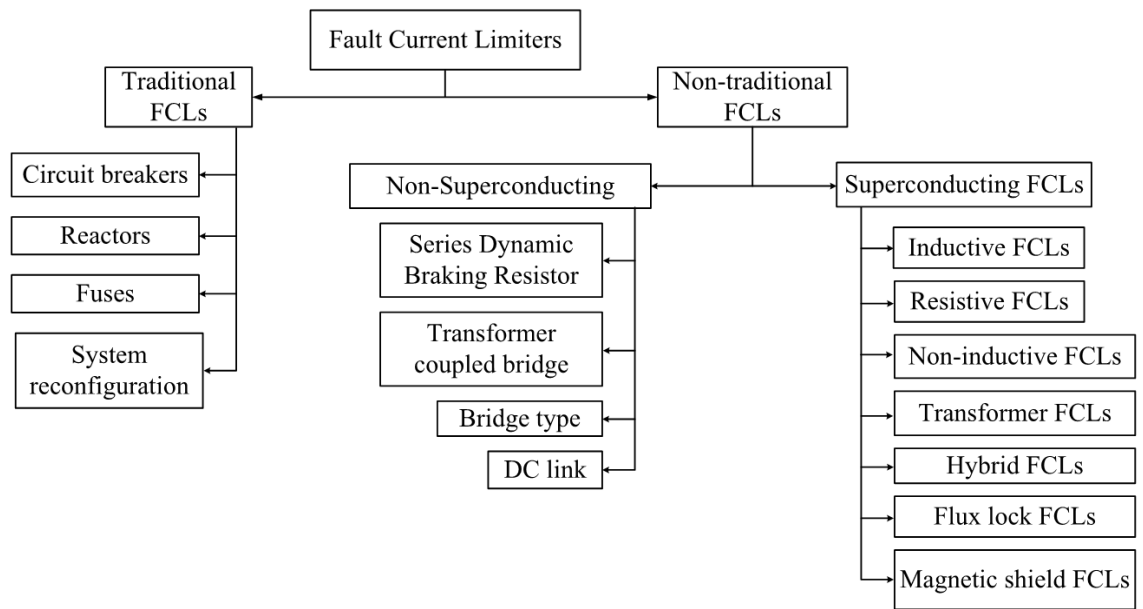
Figure 2.1. Fault current limiters classification.

Fuses are simple and reliable and used in medium and low voltage networks. Circuit breakers are a common part of a protection system. Reactors are used to increase the network impedance [12]. However, traditional FCLs have shortcomings when they are utilized in power systems. Fuses are one-time use; reactors are bulky and expensive; circuit breakers require periodic maintenance.

Non-superconducting FCLs represent better options. As the transformer-coupled bridge considered to be a better option as compared to the conventional transformers and reactors[13]. DC reactors are presented as a cost-effective FCL [14]. Diodes bridge was also proposed to hold the current magnitude through a discharging resistor in the proposed structure [15]. The Non-superconducting FCLs are also proposed to enhance the stability along with current limitations [16], [17]. But they require periodic maintenance and cause a persistent voltage drop during normal operation.

6

On the other hand, superconducting FCLs (SFCLs) cause a negligible voltage drop during normal operation. SFCLs are more advanced in technology since materials with high conductivity are used, such as Yttrium-Barium-Copper-Oxide (YBCO), and Bismuth-Strontium-Calcium-Copper-Oxide (BSCCO). The materials, as mentioned earlier, can change its conductivity from a superconducting state to a normally conducting state in a process called "quenching" [18]. Resistive type SFCL is proposed and developed in [19]. During normal conditions, the resistance is very low, opposing a high resistance during fault to limit the current. Inductive type SFCL is proposed in [20] to be placed as shorted secondary winding of a transformer. If a fault occurs, the inductive SFCL placed at the secondary winding quenches and increases the impedance to limit the current. Also, hybrid type SFCLs are proposed to overcome the problems of the SFCLs types before hybridization [21]. Even with the superior performance of SFCL, problems of a high level of complexity in design, high cost as a consequence of employing the superconducting material and cooling systems, reduced reliability, and short lifetime. Therefore, the shortcomings of FCLs drove the research toward different techniques.

2.4 Current Limitation Through Control Algorithms

An alternative way to implement FCLs is by modifying the DG controller to limit the inverter's fault current, similar to the effect of adding a physical series impedance [22]. This modification adds a virtual impedance in the DG equivalent circuit and leads to the development of VI-FCLs. The need for VI-FCLs arises to protect the inverter's switches from any thermal stress during short-circuit faults.

A protection strategy is proposed to protect the voltage source inverter against large load currents in [23]. The proposed strategy is performed by reducing the reference point

of the inverter's voltage such that the inverter acts as a voltage source behind a virtual resistance when the inverter's current exceeds a certain threshold. The analysis, design, and implementation of a VI-FCL is presented in [24]. The stability, transient response, and power flow performance of the DG are considered toward the design. The improvement of the low-voltage ride-through capability of a doubly-fed induction generator is proposed in [25]. The improvement was made through the limitation of the current by a virtual resistance when the stator of the generator is subjected to grid disturbances. Another work is done in [26] to limit the current for inverters operating in parallel with synchronous generators. The use of VI-FCL is to avoid the current saturation point, which usually leads to stability issues. In [27], VI-FCL control is proposed for microgrids powered by inverters. The VI-FCL is implemented in the inverters controller by adding a virtual impedance loop. This loop is active only during faults to control the magnitude of the voltage.

The concept of VI-FCL isn't only limited to traditional inverters but also has been applied to synchronverters. The authors of [28] propose a single-phase self-synchronized synchronverter with current-limiting capability. The proposed synchronverter can self-synchronize before the grid connection, and it limits the current during grid disturbances. The current limitation is done by controlling the synchronverter current to track a saturated reference current generated by a virtual impedance. The characteristics and restraining method are discussed in [2], in which the current is produced by a virtual impedance and limited by a hysteresis controller to track a pre-set reference current. The proposed method [29] extends the work in [28] by improving the dynamic response of the active and reactive power loops, and by allowing for current limitation using proportional-resonant (PR) controllers. In [30], the fault currents of parallel synchronverters are limited during

8

disturbances. The current control is performed by generating an indirect virtual reference value to be tracked by the inverter's output current while avoiding the loss of synchronism when the current saturates.

The existing VI-FCL control methods for synchronverters mainly focus on stability enhancement or protection of power-electronic switches. There is a gap in modeling synchronverters with VI-FCLs for the protection of ADNs, particularly, OPC studies.

2.5 Optimal Protection Coordination (OPC)

OPC is the determination of relays settings in a way to isolate faulted areas within a power system while ensuring minimum area isolation during a fault event [3]. The OPC studies have been conducted many times with different solvers, considering passive FCLs, and different relay characteristics.

In [31], the OPC problem is formulated as Mixed-Integer Nonlinear Programming (MINLP) and has been solved using the particle swarm optimization (PSO). [32] enhances the solution of the PSO algorithm using constraint handling. In [33], the objective function of the Genetic Algorithm (GA) solver is modified by adding a parameter to handle the miscoordination problem for both continuous or discrete relays settings. Other examples for solving the OPC program using different solvers to reduce the value of the objective function are presented in [34]–[41].

The proposition of using FCLs in series with DGs to restore coordination among DOCRs is proposed in [42]. First, the relay settings are obtained. Then, the FCL size is calculated to keep the coordination time between primary and backup relays within a certain limit. In [43], besides employing a hybrid GA solver, different network topologies are taken into account. In [44], the application of FCLs for the OPC of microgrids is

9

considered. This study considers an inductive FCL to be placed at the substation to reduce the incoming current from the main grid to guarantee proper coordination for the islanded and grid-connected modes of microgrid operation.

In [45], the OPC formulation incorporated time considerations specified by fault-ride-through (FRT) requirements. The OPC using a new time-current-voltage characteristic is proposed in [46]. This study considers the relay's voltage measurement in addition to the current magnitude to further minimize the objective function. In [47], the OPC problem is formulated considering dual settings for DOCRs to enhance the coordination and reduce the relay's operation time in meshed ADNs. [48] proposed a Cuckoo hybrid optimization to resolve the OPC program in [32]. The result of this study shows a significant reduction in the total operating time of all relays.

However, the effect of synchronverters on DOCRs is not analyzed, and the OPC problem was not formulated to incorporate synchronverters.

2.6 Conclusion

Synchronverters can enhance system stability but should be protected against inrush currents during faults. FCLs are required to suppress the inrush currents, but the physical FCLs aren't the best choice toward a cost-effective solution. VI-FCLs can provide a remedy by only modifying the DG controller. Besides limiting the fault current, VI-FCLs are also designed to enhance the stability and transient response. Nonetheless, VI-FCLs are not incorporated in OPC studies, especially, for ADNs powered with synchronverters. Further studies need to be conducted to incorporate VI-FCLs in short-circuit analysis and OPC studies. Also, most of the existing VI-FCLs are assumed to be fixed, which may make

the relay's current undetectable when the fault resistance is relatively high. Figure 2.2 summarizes the literature survey and highlights the shortcomings.
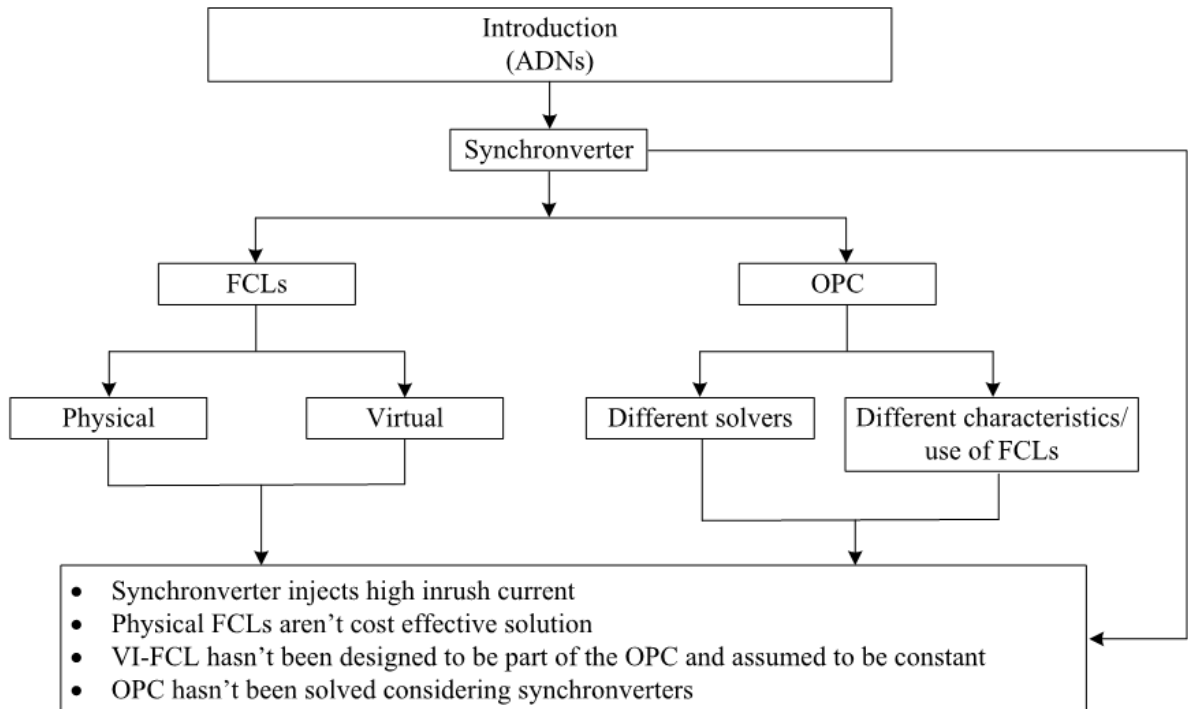
Figure 2.2. Literature survey summary.

CHAPTER 3

PRELIMINARIES

3.1 Introduction

In order to integrate synchronverters in the formulation of the OPC problem, the fundamentals of both synchronverters and OPC should be reviewed. In this chapter, the idea of operating a three-phase inverter to mimic the behavior of a synchronous generator is presented. Case studies are conducted to explain the model and control of synchronverters. Furthermore, the basic formulation of OPC based on [44] is illustrated by a case study on a 9-bus Canadian distribution network powered by four synchronverters.

3.2 Synchronverter Implementation

The synchronverter comprises two parts, the power part which injects energy into the grid and the electronic component to control the power part. The power part is a three-phase inverter, as depicted in Figure 3.1. The inverter has three legs; each leg consists of two fully controlled switches. The switches shown are insulated gated bipolar transistors (IGBTs) with their antiparallel diodes. The LC filter components are R_s, L_s, and C_s to reduce the voltage and current ripples. The power part is connected to the grid through a circuit breaker. The network is represented by a voltage source behind an impedance (L_g and R_g). On the other hand, the electronic part is responsible for regulating the real and reactive powers of the synchronverter.
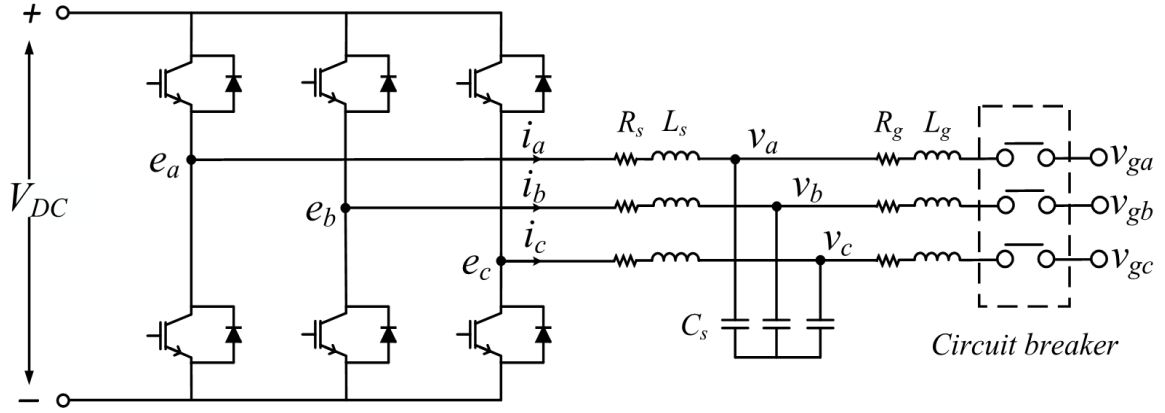
Figure 3.1. Synchronverter's power part.

The back electromotive force vector e is related to the synchronverter terminal voltage vector v through the filter impedance and the current flowing vector i. Therefore, e is given by

$$e = v + R_s i + L_s \frac{di}{dt} \tag{3.1}$$

The vectors $e, v,$ and i are defined by

$$e = [e_a\ e_b\ e_c]^T \tag{3.2a}$$

$$v = [v_a\ v_b\ v_c]^T \tag{3.2b}$$

$$i = [i_a\ i_b\ i_c]^T \tag{3.2c}$$

The e vector is generated due to the rotor movement in synchronous generators, while this rotor is virtual in synchronverters. However, the same equation holds for both

$$e = M_f i_f \dot{\theta} \widetilde{\sin} \theta - M_f \frac{di_f}{dt} \widetilde{\cos} \theta \tag{3.3}$$

During steady-state conditions, the field current i_f is constant, thus, (3.3) can be rewritten as

$$e = \dot{\theta} M_f i_f \widetilde{\sin} \theta \tag{3.4}$$

where M_f denotes the mutual inductance. The terms $\widetilde{\sin}\,\theta$ and $\widetilde{\cos}\,\theta$ represent balanced sinusoidal functions:

$$\widetilde{\sin}\,\theta = \left[\sin\theta \ \ \sin\left(\theta - \frac{2\pi}{3}\right) \ \ \sin\left(\theta - \frac{4\pi}{3}\right)\right]^T \tag{3.5a}$$

$$\widetilde{\cos}\,\theta = \left[\cos\theta \ \ \cos\left(\theta - \frac{2\pi}{3}\right) \ \ \cos\left(\theta - \frac{4\pi}{3}\right)\right]^T \tag{3.5b}$$

Therefore, the electromotive force vector e can be expressed as

$$e = E\,\widetilde{\sin}\,\theta \tag{3.6}$$

where E is the magnitude of the electromotive force. The active and reactive powers are defined by

$$P = \dot{\theta}M_f i_f \langle i, \widetilde{\sin}\,\theta \rangle \tag{3.7a}$$

$$Q = -\dot{\theta}M_f i_f \langle i, \widetilde{\cos}\,\theta \rangle \tag{3.7b}$$

where $\dot{\theta}$ is the angular frequency, which is governed by the acceleration of a synchronous generator:

$$\dot{\theta} = \frac{1}{J}\int \left(T_m - T_e - D_p\left(\dot{\theta}^* - \dot{\theta}\right)\right) dt \tag{3.8}$$

where J is the moment of inertia for a synchronous generator; here, it is called the virtual inertia. T_m is equivalent to the mechanical torque of a synchronous generator. In a synchronverter, T_m is defined as a function of the active power set point P_{set} and the grid nominal frequency $\dot{\theta}_n$, i.e.,

$$T_m = \frac{P_{set}}{\dot{\theta}_n} \tag{3.9}$$

14

In (3.8), T_e represents the electromagnetic torque of the synchronverter. It is proportional to the active power given in (3.7a), i.e.,

$$T_e = M_f i_f \langle i, \widetilde{\sin} \, \theta \rangle \tag{3.10}$$

Referring to (3.8), D_p is the frequency droop coefficient. D_p regulates the droop relation between active power and grid frequency. D_p drives the synchronverter to generate an incremental real power for every drop incremental in grid frequency, i.e.,

$$D_p = -\frac{\Delta T}{\Delta \dot{\theta}_n} \tag{3.11}$$

Since the synchronverter has a virtual inertia J, it can be controlled based on the time constant of the frequency loop τ_f and D_p as follows:

$$J = D_p \tau_f \tag{3.12}$$

Another power loop is associated with the reactive power Q, which is regulated with respect to the measured terminal voltage. The reactive power generation Q can be controlled through $M_f i_f$ by choosing a proper D_q droop coefficient which affects defined later reactive power regulating factor K. the term $M_f i_f$ is defined as

$$M_f i_f = \int \frac{1}{K} \Big(Q_{set} - Q + D_q \big(E^* - V_g \big) \Big) dt \tag{3.13}$$

where V_g is the magnitude of the terminal voltage, E^* is the magnitude of the reference voltage, Q_{set} is the reactive power setpoint, D_q is the $Q–V$ droop coefficient, K is the reactive power regulating factor. D_q drives the synchronverter to inject an incremental reactive power corresponding to an incremental drop in the terminal voltage as given by

$$D_q = -\frac{\Delta Q}{\Delta V_g} \tag{3.14}$$

K depends on the time constant of the voltage loop τ_v and D_q, i.e.,

$$K = D_q \tau_v \dot{\theta} \tag{3.15}$$

Figure 3.2 shows the block diagram that includes the synchronverter's model and controller in (3.2)–(3.15). The droop characteristics of the synchronverter allow reliable operation when it is grid-connected or standalone [1].
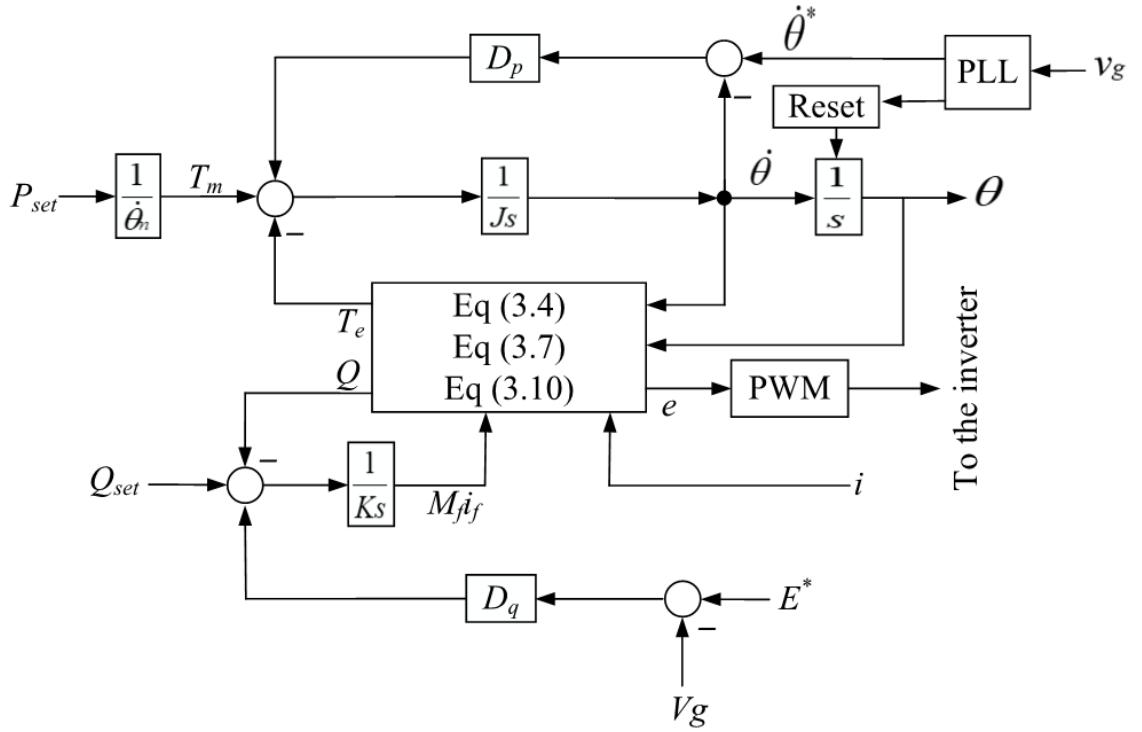
Figure 3.2. Synchronverter's Control algorithm diagram.

3.3 Synchronverter Simulation

The synchronverter model is simulated in this section when it is connected to a grid to demonstrate the power tracking mechanism. The model is built in MATLAB/Simulink, and it follows the mathematical model described in Section 3.2. It is worth noting that the

16

simulated model is developed in per unit (p.u.) so that it can be easily integrated into distribution networks at different voltage levels and power ratings. Table 3.1 displays the synchronverter parameters used for simulation.

Table 3.1. Synchronverter's simulation parameters.

Parameter	Value	Parameter	Value
S_{base}	4 MVA	τ_f	0.002 s
P_{set}	3.6 MW	τ_v	0.02 s
Q_{set}	1.74 MVAR	V_{DC}	784 V
E^*	480 V	f	60 Hz
R_s	0.003 Ω	R_g	0.0014 Ω
L_s	0.004 mH	L_g	0.0013 mH

Figure 3.3 shows the simulated systems, in which, the power part of the synchronverter is simulated by the average model of a three-phase inverter, and the grid is modeled by a voltage source behind an impedance.
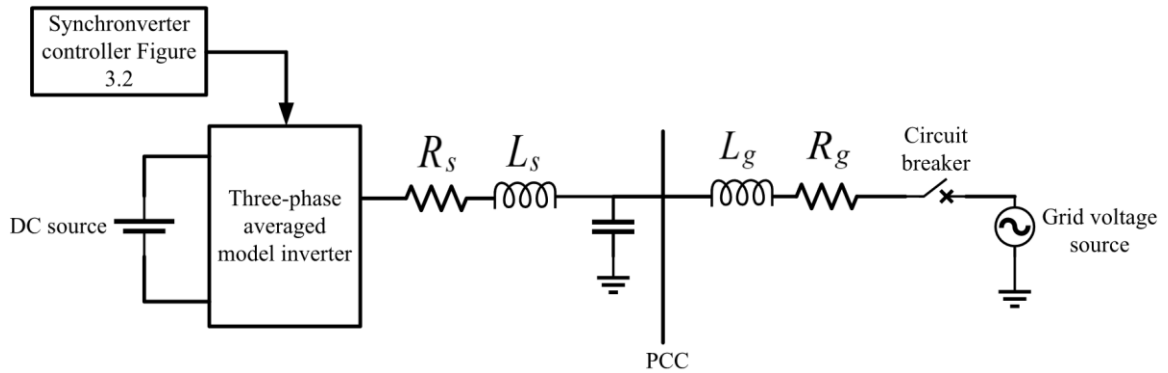
Figure 3.3. Synchronverter's simulation model.

In that model, D_p is calculated to drive the synchronverter to generate 100% of the real power for every 5% drop in the grid's frequency. On the other hand, D_q is chosen to

drive the synchronverter to generate 100% of reactive power for every 10% drop in the grid's voltage magnitude.

The nominal setpoints for active and reactive powers are 0.9 p.u. and 0.4359 p.u., respectively. To check the active and reactive power tracking, the grid frequency and voltage are changed.

As shown in Figure 3.4(a), the grid frequency is dropped to 57 Hz between $t = 0.5$ s and 0.7 s, i.e., 5% frequency variation. It can be seen that the active power tracks the setpoint accurately when the frequency is 60 Hz, as shown in Figure 3.4(b). During the frequency disturbance, the active power jumped to 1.8 p.u. due to the droop characteristics. 5% drop in the frequency corresponds to 100% active power increase, and that why the active power increases from 0.9 p.u. to 1.8 p.u. Nonetheless, the reactive power is not impacted by the changes in the frequency, as shown in Figure 3.5(c). Figures 3.5(d) and (e) display the corresponding changes in the back EMF and output current.
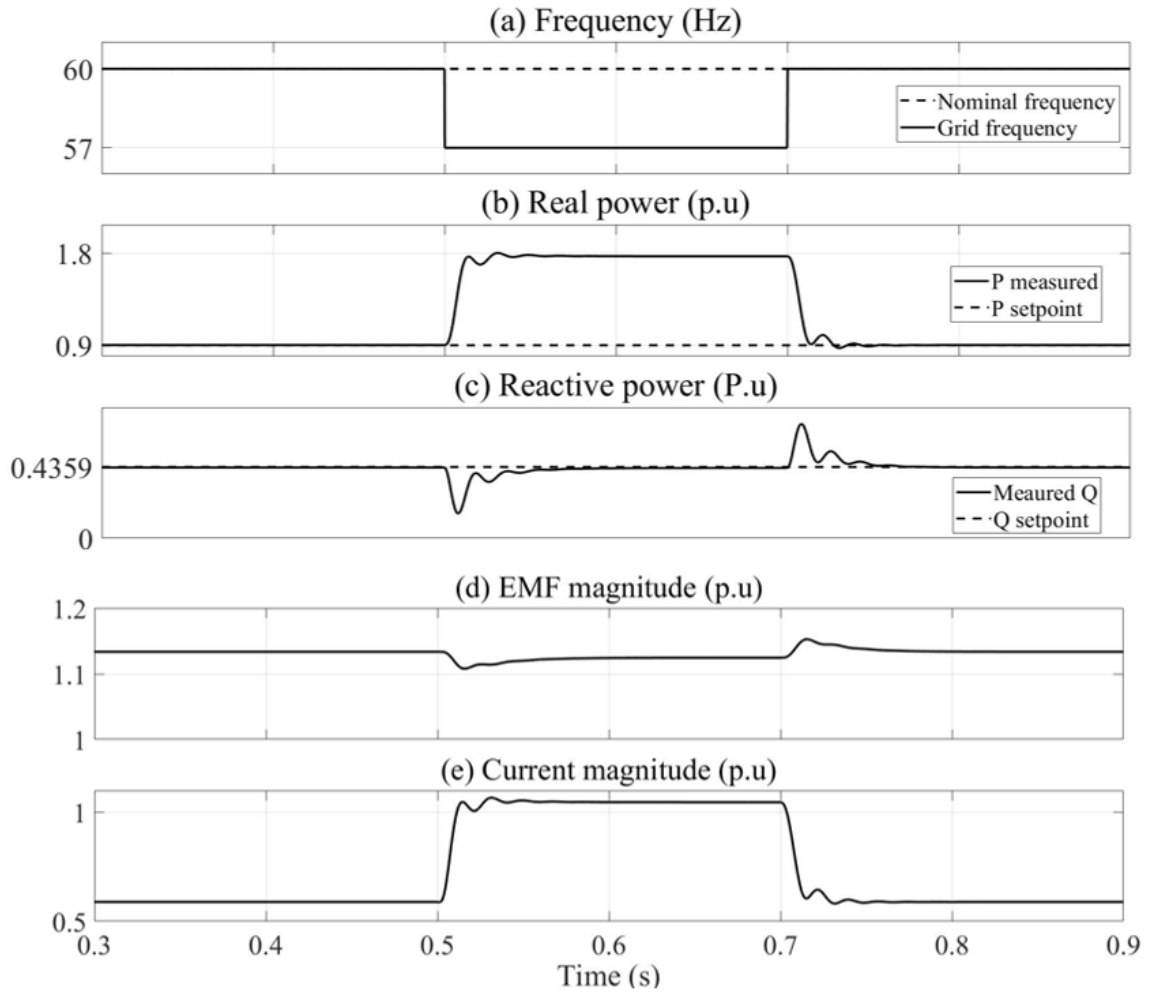
Figure 3.4. Synchronverter response to 5% frequency drop.

The operation of the $Q–V$ droop characteristic is assessed by varying the grid voltage. As shown in Figure 3.5(a), the grid voltage magnitude is dropped to 0.9 p.u. between $t =$ 0.5 s and 0.7 s, i.e., 10% magnitude variation. It can be seen that the reactive power tracks the setpoint accurately when the magnitude is 1.0 p.u. as shown in Figure 3.5(b). During the voltage drop, the reactive power jumped to 0.88 p.u. due to the $Q–V$ droop characteristic 10% drop in the voltage magnitude corresponds to a 100% reactive power increase, i.e., 0.44 p.u. additional reactive power. However, the active power is not impacted by the changes in the voltage, as shown in Figure 3.5(c). Figures 3.5(d) and (e) display the changes

in the back EMF and output current as a result of the voltage drop. E is increased as a result of the reactive power increase. This happens because both E and Q are proportional $M_f i_f$.
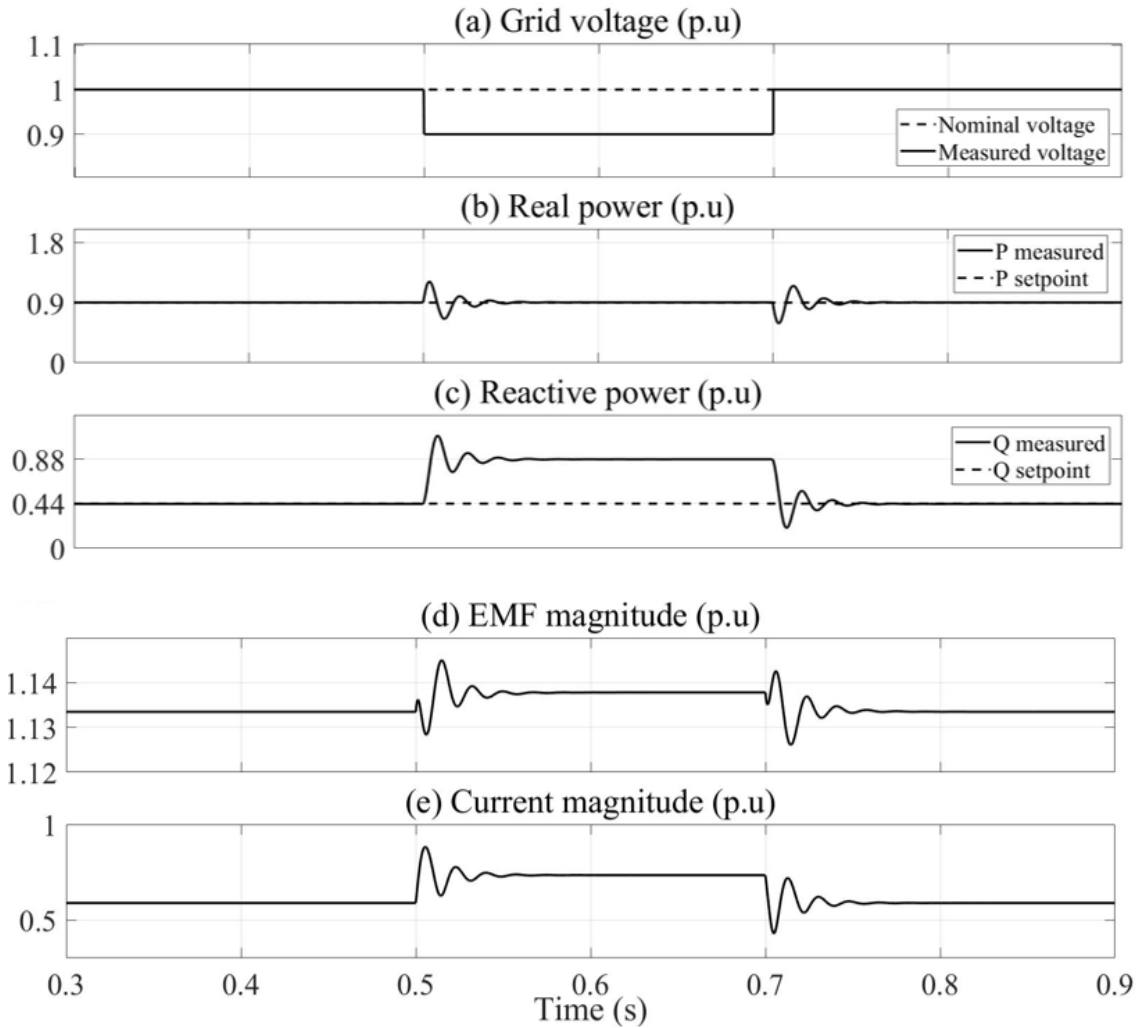
Figure 3.5. Synchronverter's response during a 10% magnitude drop.

3.4 Protection Coordination of Directional Overcurrent Relays

DOCRs are typically used for distribution network protection. They respond to the magnitude and direction of fault currents. As the magnitude of the fault current increases, a DOCR reacts faster [3]. OPC of DOCRs is the process of selecting proper primary-and-backup relay sets and adjusting the relays' settings to minimize the total operating time and ensure minimum isolation of a faulted area.

20
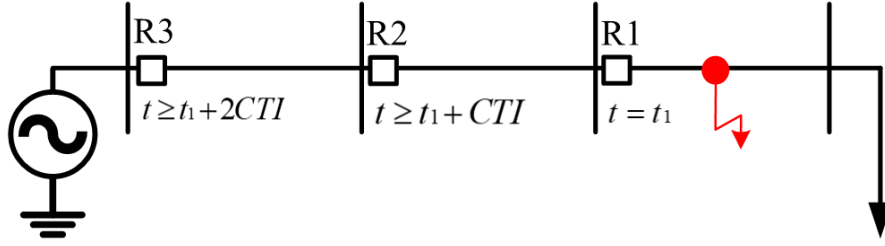
Figure 3.6. Protection coordination of a simple radial system.

Figure 3.6 is used to elaborate on how to select primary-and-backup relay sets. The red dot and arrow refer to the fault location. The fastest relay to operate should be the closest to the fault location, i.e., R_1. If it doesn't work, R_2 should act after an intentional time delay as a backup for R_1. This delay is known as the coordination time interval (CTI). Likewise, R_3 is the backup for R_2 with double the CTI between R_1 and R_2.

The objective of the OPC is to minimize the total operating time for all relays to guarantee fast fault isolation while considering CTI to ensure coordination. In this thesis, the OPC program is formulated based on [44]. The objective function is to minimize the summation of the operating times of all primary and backup relays as

$$min\, T = \sum_{n=1}^{NR} \sum_{j=1}^{NF} (t_{nj}^{p} + \sum_{k=1}^{NB} t_{njk}^{bk}) \tag{3.16}$$

where NR is the total number of relays, NF is the total number of fault locations, n and j are indices for relays and fault locations, respectively, and NB the number of backup relays associated with each primary relay with k denoting the backup relay identifier. Each primary relay may have one or more backup relays. The superscripts p and bk stand for the primary and backup relay, respectively. The DOCRs typically adopt inverse-time characteristics that are given by

$$t = TDS \frac{A}{\left(\frac{I_f}{I_p}\right)^B - 1} \tag{3.17}$$

where TDS is the time dial settings, A and B are constants that define the relay characteristics, and I_f is the magnitude of the fault current measured by the relay, and I_p is the relay's pickup current. I_p should be higher than the relay's nominal current (during normal conditions) by a margin, for instance, 25% or more. The decision variables of this optimization program are I_p and TDS and are subjected to the following bounds:

$$I_{p_{min}}^{(n)} \leq I_p^{(n)} \leq I_{p_{max}}^{(n)} \qquad \forall n \tag{3.18a}$$

$$TDS_{min}^{(n)} \leq TDS^{(n)} \leq TDS_{max}^{(n)} \qquad \forall n \tag{3.18b}$$

A set of nonlinear constraints is imposed to ensure a minimum operating gap between each primary relay and its backup (CTI) as follows:

$$t_{njk}^{bk} - t_{nj}^{p} \geq CTI \qquad \forall n, \{j, k\} \tag{3.19}$$

3.5 OPC for a Canadian Test System

The OPC is performed for a 9-bus test system power with four synchronverters based on a Canadian distribution network [49], as shown in Figure 3.7. The system encompasses eight loads and four synchronverters. Each load is rated at 2 MVA with 0.9 lagging power factor. Each synchronverter is 4 MVA and is interfaced to the grid through a 480V/12.47kV transformer. The transformer impedance is 10%. Balanced faults (f10 – f17) are applied at the midpoints of the lines, as indicated by the red dots.
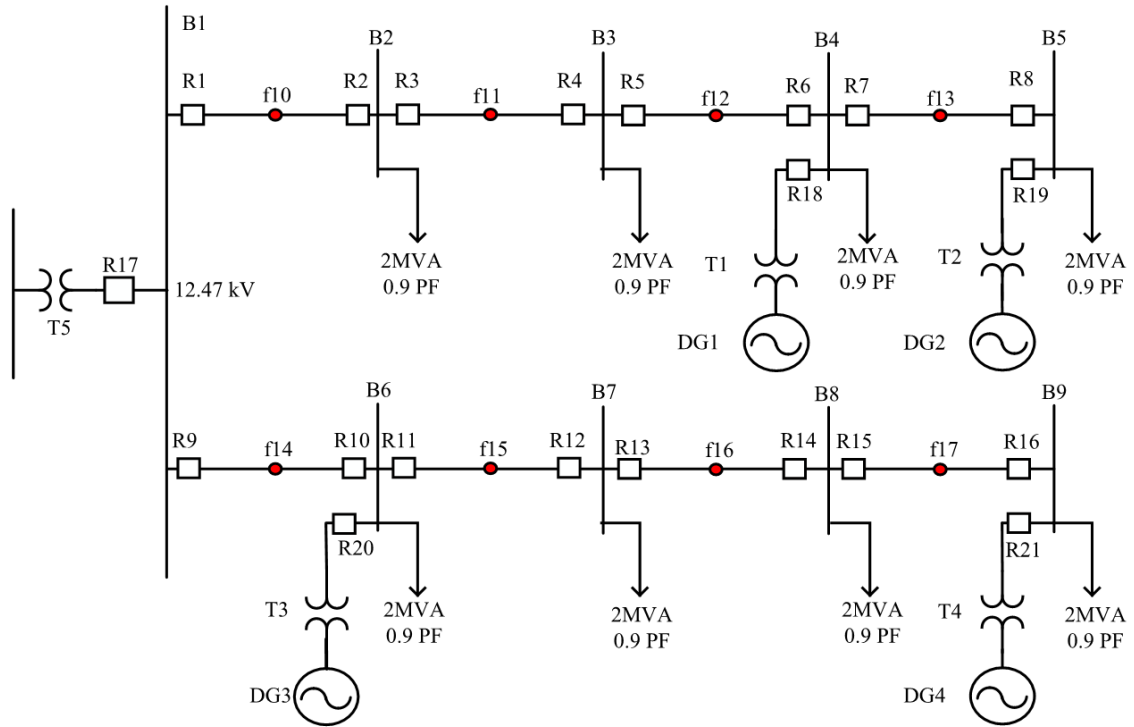
Figure 3.7. Schematic diagram of the 9-bus test system.

To calculate the short-circuit currents through the relays, a circuit model for the synchronverters should be adopted. Since a synchronverter imitates the behavior of an SG, a voltage source model is used to represent synchronverters in short-circuit current calculations. The details of that model with VI-FCLs will be explained in Chapter 5. The OPC program is solved using the GA. The GA is used since the problem is highly nonlinear. Thus, using an exact solver make may not guarantee optimality [50]. Solving the OPC program results in a total operating time of 25.5065s. The optimal settings for each relay are displayed in Table 3.2.

Table 3.2. Relays optimal settings to minimize their operating times.

Relay	$TDS(s)$	I_p $(p.u.)$	Relay	$TDS(s)$	I_p $(p.u.)$
1	0.1421	1.3666	12	0.0980	1.2500
2	0.1258	1.2501	13	0.0591	1.2500
3	0.0983	1.2501	14	0.1060	1.3639
4	0.1409	1.4956	15	0.0100	1.2500
5	0.0510	1.2500	16	0.1368	1.2500
6	0.1999	1.2501	17	0.2800	0.6250
7	0.0101	1.2500	18	0.2893	0.6251
8	0.1327	1.2500	19	0.3083	0.6255
9	0.1413	1.2505	20	0.2264	0.6251
10	0.1435	1.2500	21	0.3137	0.6256
11	0.1106	1.2920			

Based on Table 3.2, the relay's operating times are calculated as in Table 3.3. As can be seen, the CTI constraints are preserved, i.e., the time gap between each primary relay and its backup is greater than or equal to 0.2s. These results confirm the successful implementation of the OPC program in a distribution network powered by synchronverters.

Table 3.3. Operating times of primary-backup sets corresponding to their faults.

Fault	P_1	B_{11}	B_{12}	P_2	B_{21}	B_{22}
f10	R1 0.5091	R10 0.709	R17 0.7083	R2 0.6201	R4 0.8192	
f11	R3 0.3701	R1 0.5691		R4 0.7409	R6 0.9403	
f12	R5 0.2092	R3 0.4085		R6 0.8584	R8 1.0577	R18 1.0577
f13	R7 0.049	R5 0.2352	R18 1.0577	R8 0.9341	R19 1.1338	
f14	R9 0.5040	R2 0.7033	R17 0.7083	R10 0.6249	R12 0.8246	R20 0.8241
f15	R11 0.3713	R9 0.5703	R20 0.8241	R12 0.7268	R14 0.9263	
f16	R13 0.2160	R11 0.4150		R14 0.8459	R16 1.0449	
f17	R15 0.0400	R13 0.2390		R16 0.9716	R21 1.1611	
T = 25.5065 s						

CHAPTER 4

PROBLEM STATEMENT

4.1 Introduction

The overall shortcomings in Chapter 2 motivate the work of this thesis as follows:

- A synchronverter model has to be adopted for the purpose of short-circuit current calculations and OPC studies.

- There is a need to develop a current limiter that ensures safe and reliable operation of synchronverters and keep their models at different fault conditions intact.

- A new formulation for OPC studies that include synchronverters with current limiters is needed without adding complexity.

In this chapter, the problem of inrush currents from synchronverters is demonstrated, and VI-FCLs are promoted as a remedy. Besides, issues related to unified OPC schemes are explained.

4.2 Synchronverter Inrush Current

The synchronverter modeling for the fault current calculation purposes was studied for balanced faults [2] and unbalanced faults [51]. Both studies modeled the synchronverter as a voltage source, as supported by (3.4) and (3.6). A synchronverter can be modeled as a voltage source behind an impedance, as illustrated in Figure 4.1.
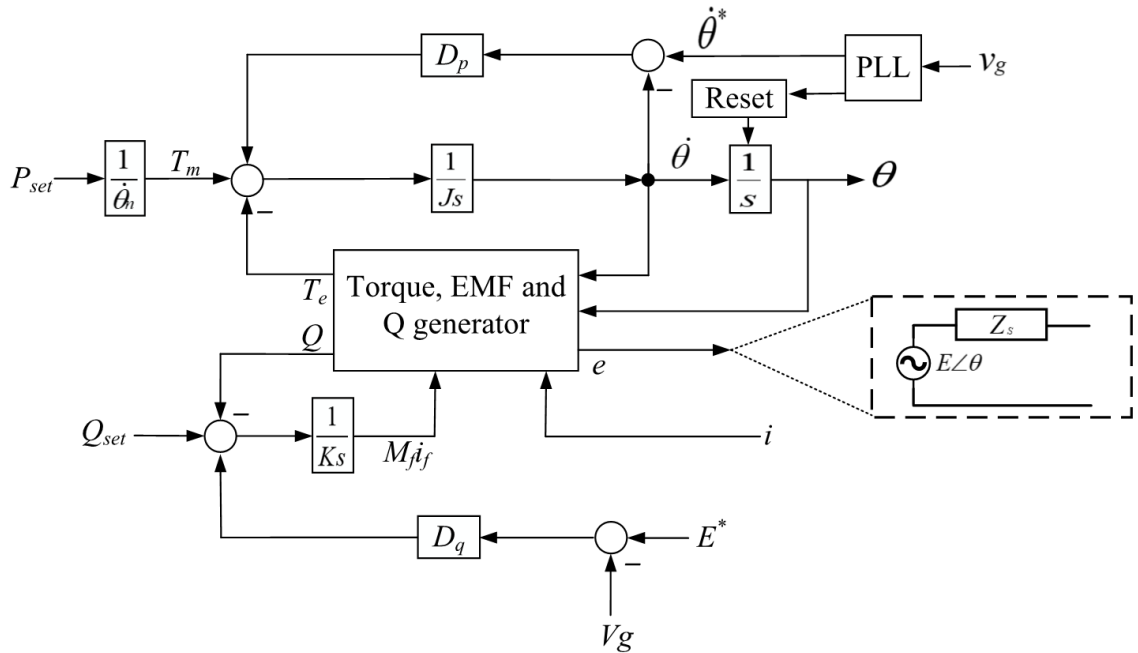
Figure 4.1. Synchronverter's voltage source model.

Because of the nature of the voltage source model and the absence of a current limiter, a synchronverter may inject high inrush current during faults. To demonstrate this problem, a bolted fault is applied at the point of common coupling (PCC) of the test system shown in Figure 4.2. The fault current from the synchronverter is above three times the inverter's rated current are displayed in Figure 4.3.
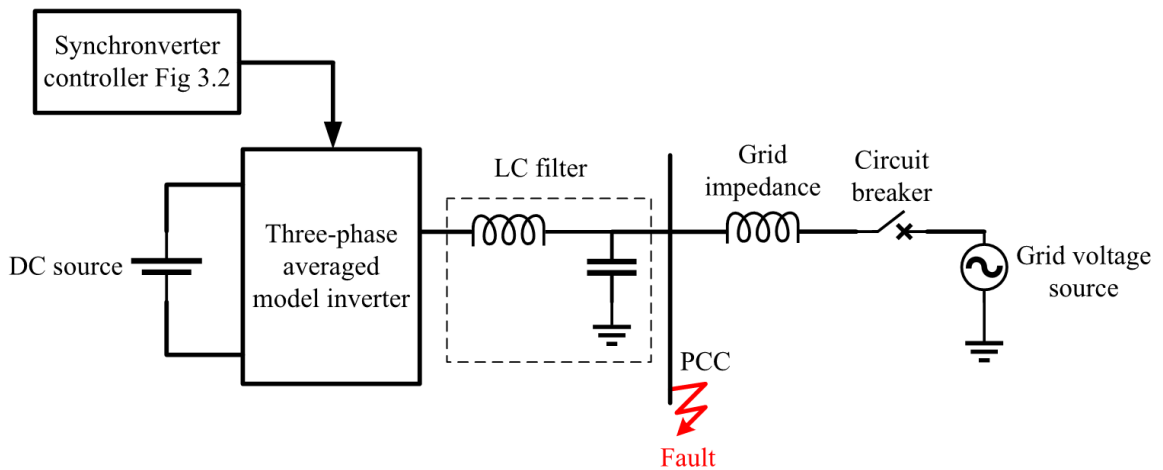
Figure 4.2. Grid-synchronverter test system with a fault at the PCC.

27
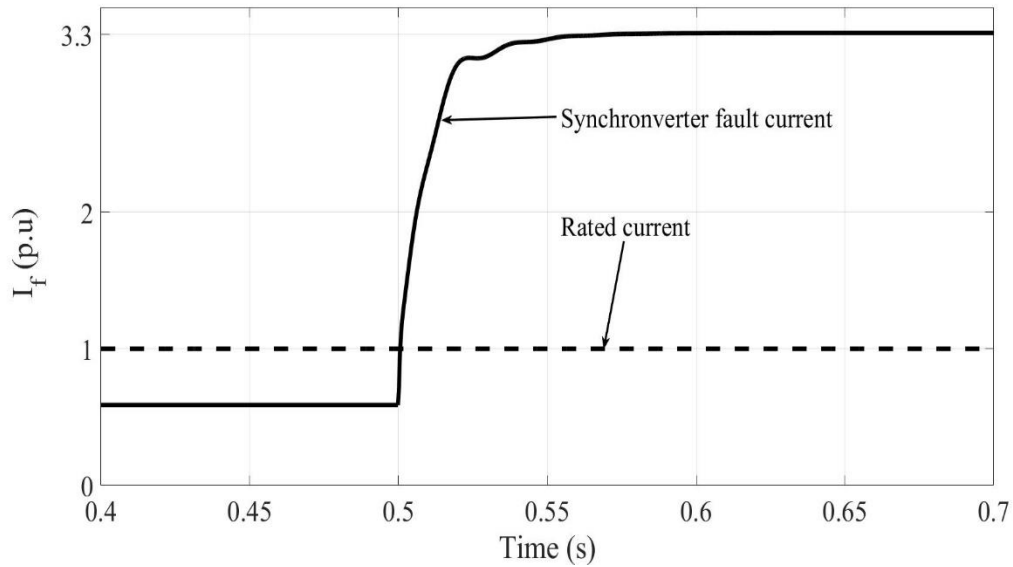
Figure 4.3. Synchronverter fault current during a balanced fault.

A possible way to limit the current is by adding a hard limiter, which will make the synchronverter behaves as a current source [28]. Figures 4.4 and 4.5 illustrate how a current limiter can be added to the synchronverter controller. Dividing the voltage difference between the generated EMF e and the terminal voltage v_t by the filter, impedance obtains a reference value for the inverter's output current. This value is then transformed to the synchronously rotating reference frame (dq) using Park's transformation to deal with dc quantities, which can be limited. A PI controller ensures that the limited reference current is tracked. The output of the PI controller is added to the dq components of v_g, which provides a feed forward compensation, to generate the new EMF e' that results in a limited current during faults. Finally, the added terms are transformed back to abc to generate the PWM signals that trigger the inverter.
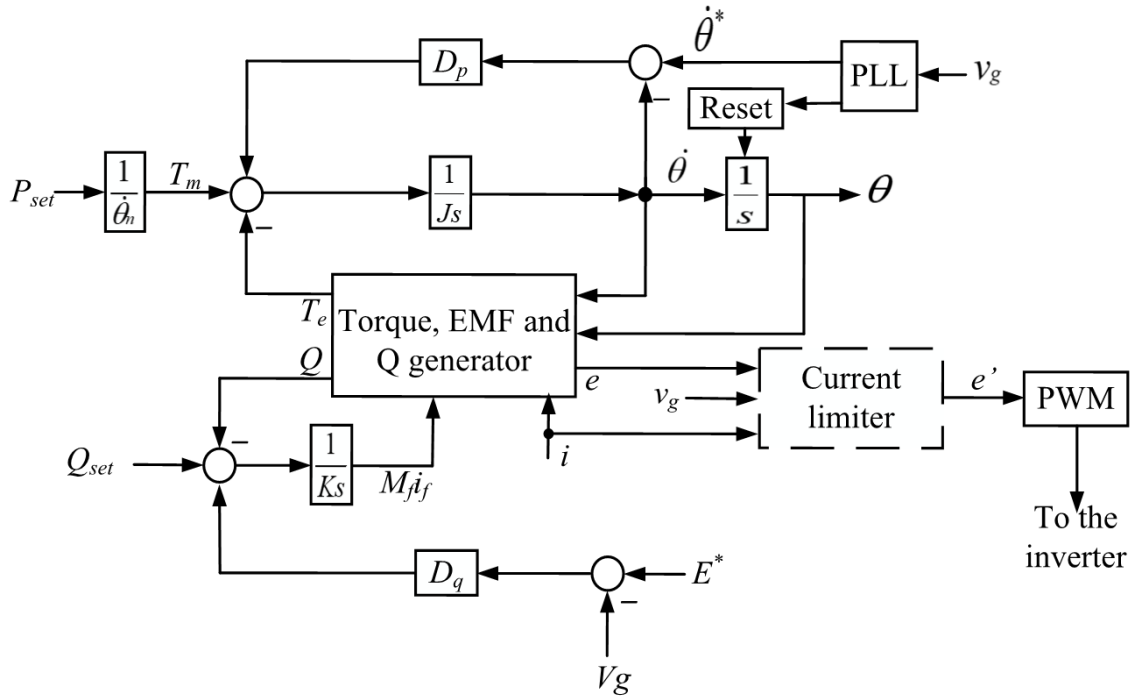
Figure 4.4. Synchronverter controller with hard current limiting.
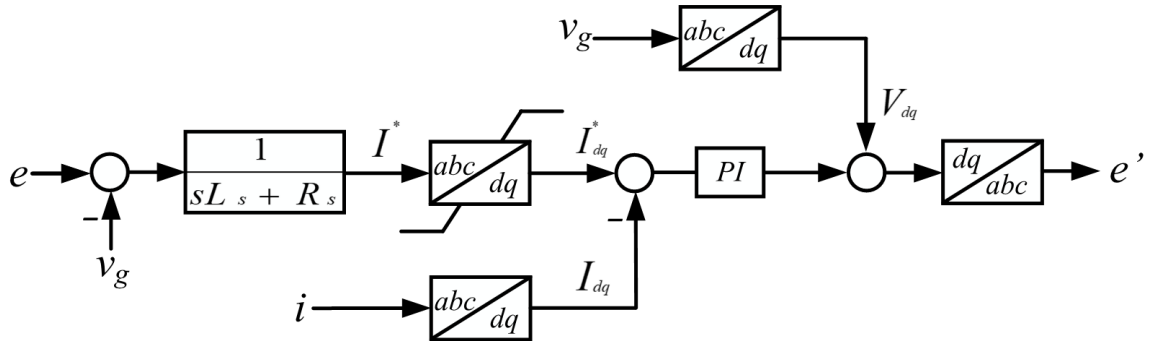
Figure 4.5. Current limiting controller.

Time-domain simulation is carried out to examine the feasibility of the hard limiter that was added to the original model of the synchronverter. Figure 4.6 shows that the inverter's current could be successfully limited to 1.5 p.u. after the fault inception at $t = 0.5$ s.
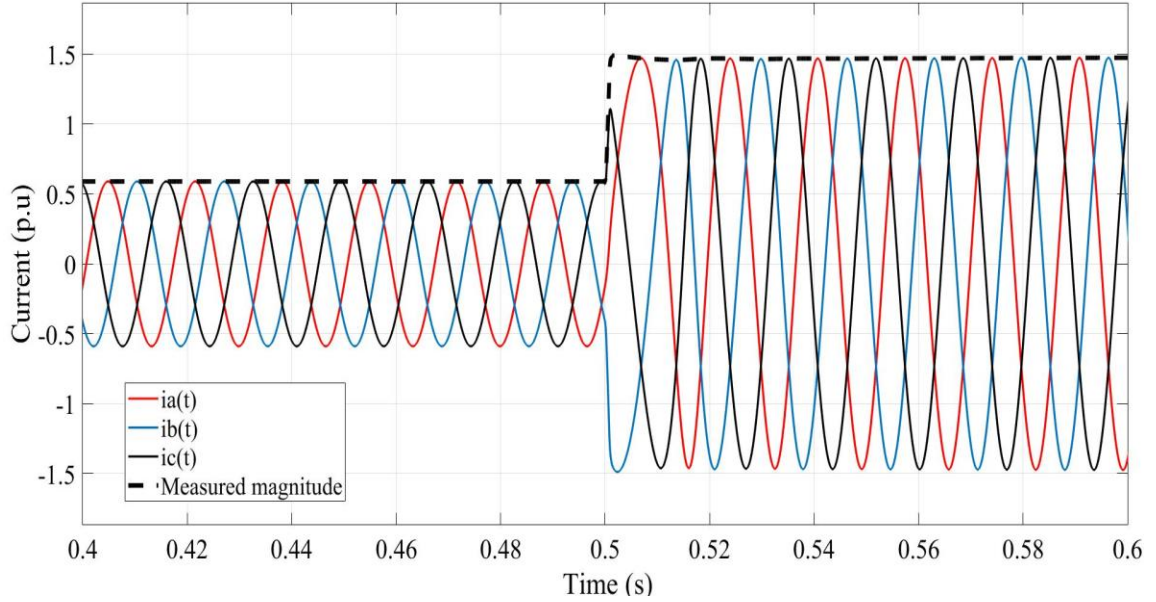
Figure 4.6. Synchronverter's saturated current during a balanced fault event.

However, the use of hard current limiters may make the OPC problem infeasible to solve because the fault current from inverters will not be sensitive to fault location and resistance. Thus, a suitable fault current limiting technique should be developed to keep the reliable operation of DOCRs. It is therefore proposed to limit the fault current from synchronverters using VI-FCLs.

4.3 OPC Formulation

The OPC formulation is extended to determine the magnitudes of VI-FCLs that keep the current within desired limits and keep the voltage source model intact. This formulation is similar to the one done in Chapter 3, but it has constraints on the VI-FCL parameters, which are formulated in terms of the fault currents to be limited. The objective function to be minimized is given (3.16) with the time-current characteristic defined in (3.17). Also, the relays settings are subjected to the bounds in (3.18) and (3.19). The VI-FCLs are

incorporated in the OPC through the magnitude of the inverter's fault current I_f, which is defined for each synchronverter by

$$I_f^{(d)} = \frac{(E - V_f)^{(d)}}{Z_{FCL}^{(d)}} \tag{4.1}$$

where d is the synchronverter identifier, E is the magnitude of the EMF, V_f is the measured terminal voltage during faults, and $Z_{FCL}^{(d)}$ is the magnitude of the VI-FCL impedance, which is bounded as follows:

$$Z_{FCL\,min}^{(d)} \leq Z_{FCL}^{(d)} \leq Z_{FCL\,max}^{(d)} \qquad \forall d \tag{4.2}$$

A set of nonlinear constraints is imposed to ensure the current levels are less than 150% of the rated current, i.e.,

$$I_f^{(d)} \leq 1.5 \; p.u. \tag{4.3}$$

Likewise, the GA is used to solve the OPC program with VI-FCLs. Table 4.1 shows the optimal relays' settings obtained using the unified formulation. The probability of returning a feasible solution is low. Besides the time elapsed to return, a feasible solution is long. The program is run in a loop to solve the OPC problem. Whenever a feasible solution is detected, the program terminates. This usually takes a few hours to obtain a feasible solution.

This problem could be alleviated if a good initial guess is used and when relaxing the fault current constraint in (4.3). However, using a good initial guess may not be an available option, especially when dealing with many decision variables. Also, relaxing the fault

current constraint may result in a higher inverter's fault current, which could damage the synchronverter.

Table 4.1 Relays optimal settings obtained from the unified OPC.

Relay	TDS(s)	I_p (p.u.)	Relay	TDS(s)	I_p (p.u.)
1	0.1458	1.2500	12	0.0694	1.2500
2	0.1565	1.2500	13	0.1614	1.2500
3	0.0981	1.2500	14	0.0200	1.2564
4	0.2010	1.2500	15	0.1938	1.2500
5	0.0538	1.2525	16	0.2947	1.2500
6	0.2497	1.2501	17	0.0279	0.6251
7	0.0200	1.2500	18	0.0262	0.6251
8	0.1865	1.2501	19	0.0225	0.6370
9	0.1299	1.2500	20	0.0306	0.6251
10	0.1817	1.2500	21	0.0694	0.6250
11	0.1183	1.3421			

The reason behind the solution infeasibility is related to the DGs protection relays (R18 – R21). The magnitude of the fault currents measured by the DG relays are functions of the VI-FCL values, which are, in turn subjected to bounds and nonlinear constraints. Unlike the traditional OPC formulation in Chapter 3, the unified OPC formulation mandates performing short-circuit current calculations for every set of VI-FCLs and at each fault location. Thus, the problem becomes highly nonlinear. This leads to a relatively higher execution time and the global optimal solution is less likely to be obtained. Tables 4.2 and 4.3 show the operating times of the relays and the sizes of VI-FCLs that correspond to the relays' settings in Table 4.1.

Table 4.2 Operating times of the 9-bus system relays using unified formulation.

Fault	P_1	B_{11}	B_{12}	P_2	B_{21}	B_{22}
f10	R1 0.5368	R10 0.7361	R17 0.7360	R2 0.6581	R4 0.8573	
f11	R3 0.3942	R1 0.5934		R4 0.7782	R6 0.9777	
f12	R5 0.2342	R3 0.4333		R6 0.8814	R8 1.0809	R18 1.0806
f13	R7 0.0673	R5 0.2663	R18 1.0806	R8 0.9491	R19 1.1493	
f14	R9 0.5290	R2 0.7282	R17 0.7360	R10 0.6600	R12 0.8595	R20 0.8604
f15	R11 0.4026	R9 0.6020	R20 0.8604	R12 0.7524	R14 0.9514	
f16	R13 0.2520	R11 0.4513		R14 0.8746	R16 1.0742	
f17	R15 0.0795	R13 0.2789		R16 0.9865	R21 1.187	
T = 26.6166 s						

Table 4.3 VI-FCLs magnitude obtained from the unified formulation.

Synchronverter' location	$Z_{FCL}(p.u.)$
4	0.1828
5	0.1825
6	0.1822
9	0.1809

As the fault current limit is lowered, it becomes more difficult to obtain values for VI-FCLs that guarantee a feasible solution. For example, sizing VI-FCLs to limit the fault current at 1.3 p.u. increases the probability to return an infeasible solution as compared to 2.6 p.u. It is worth noting that the unified OPC formulation adopts an approximate synchronverter model for short circuit current calculations, i.e., a voltage source behind an impedance. The

angle of the voltage source is zero. If a more accurate model is employed, such as the model in [2], the unified OPC program could take longer time to return a feasible solution or it may fail to obtain one.

Another problem encountered is related to the DG control scheme. As explained earlier in section 4.2, the synchronverter fault current can be saturated to a specific limit. Thus, the synchronverter becomes a current source. The current source DG model ensures constant current generation during regular operation as well as during faults. However, it is desired to have DGs controlled as a voltage source to support the grid's voltage during disturbances. Having a synchronverter controlled as a current source may cause miscoordination, affect the reliable and secure operation of the DOCRs, and result in faults spreading.

Table 4.4 shows the operating times of DOCRs in the 9-bus system after remodeling DG1 and DG3 are as current sources. These DGs inject their rated currents (1.0 p.u.) during faults. Also, R18 is the DOCR associated with DG1, and R20 is the DOCR associated with DG3. DG2 and DG4 are modeled as voltage sources, and their current injection is related to their operating condition. The DOCRs usually have pickup currents at least 25% higher than their nominal current. If a bolted fault occurs near DG2 or DG4, the fault condition stimulates the DG to generate current more elevated than its rated value and also higher than the pickup current of the associated DOCR. Therefore, the DOCR operates as intended and results in limited fault spreading.

On the other hand, if a bolted fault occurs near DG1 or DG3. The DG maintains its rated current generation during fault conditions due to its control scheme. The DOCR

associated with this DG may not operate properly, as demonstrated by the negative times in Table 4.4. This happens because the DOCR cannot detect a fault condition when the DG current is limited to a value less than the pickup current. As a consequence, the DG keeps supplying the grid with a fault current near its rated current, which reduces the grid efficiency and may cause a fault spreading.

Table 4.4 Operating times of the 9-bus system after remodeling DG1 and DG3.

Fault	P_1	B_{11}	B_{12}	P_2	B_{21}	B_{22}
f10	R1 0.5368	R10 0.7361	R17 0.7360	R2 0.6581	R4 0.8573	
f11	R3 0.3942	R1 0.5934		R4 0.7782	R6 0.9777	
f12	R5 0.2342	R3 0.4333		R6 0.8814	R8 1.0809	R18 **-0.8763**
f13	R7 0.0673	R5 0.2663	R18 **-0.8763**	R8 0.9491	R19 **1.1493**	
f14	R9 0.5290	R2 0.7282	R17 0.7360	R10 0.6600	R12 0.8595	R20 **-0.7085**
f15	R11 0.4026	R9 0.6020	R20 **-0.7085**	R12 0.7524	R14 0.9514	
f16	R13 0.2520	R11 0.4513		R14 0.8746	R16 1.0742	
f17	R15 0.0795	R13 0.2789		R16 0.9865	R21 **1.187**	

Therefore, the synchronverter should be equipped with a VI-FCL to limit its fault current and keep its voltage source model intact, thus avoiding the shortcomings of the current source model. Further, an OPC scheme has to be developed to prevent the problems associated with the unified OPC program while accurately calculating synchronverters' fault currents.

CHAPTER 5

PROPOSED TWO-STAGE OPC SCHEME INTEGRATING VI-FCLs

5.1 Introduction

In this chapter, the integration of VI-FCLs within the synchronverter controller is illustrated. It is proposed to use VI-FCLs with synchronverters to keep their voltage source model intact. This model can be easily incorporated in the OPC program and guarantee feasible solutions. A two-stage OPC algorithm is developed to determine the relays' optimal settings and VI-FCL parameters. Simulation results confirm the effectiveness of the proposed algorithm and promote it as a cost-effective solution toward the reliable protection of ADNs.

5.2 Proposed VI-FCL Controller

Figures 5.1 and 5.2 demonstrate the proposed VI-FCL controller. There are two steps to include a VI-FCL in synchronverter's model. First, R_s and L_s (that represent the filter's parameters) have to be enlarged to include the VI-FCL's resistance and inductance. When a balanced fault occurs at the synchronverter's terminals, i.e., the worst-case scenario, the magnitude of the fault current can be calculated using

$$I_f^{(d)} = \frac{(E - V_t)^{(d)}}{\sqrt{(R_s')^2 + (\omega L_s')^2}} \tag{5.1}$$

where R_s' and L_s' are the enlarged resistive and inductive components that include VI-FCL impedance parameters. During faults, R_s' and L_s' should replace R_s and L_s. Second, the setpoints of the real and reactive powers should be given in terms of the limited fault current. Holding the setpoint of the real power at the prefault value, while the VI-FCL is active, increases the virtual acceleration defined in (3.8). This happens due to the drop in

T_e during the fault, which makes the term $(T_m - T_e)$ higher than zero, thus, increasing the virtual acceleration. On the other hand, keeping the setpoint of the reactive power constant at the prefault value makes it higher than Q. This leads to higher $M_f i_f$, and consequently, E. The fault current from the inverter could exceed its limit even when the VI-FCL is active. Therefore, it is proposed to set the reference values of the real and reactive powers as follows

$$P_f = \frac{3}{2} E I_d \tag{5.2}$$

$$Q_f = \frac{3}{2} E I_q \tag{5.3}$$

where I_d and I_q are the dq components of the synchronverter's current during faults. The setpoints in (5.2) and (5.3) are given in terms of the limited current dq components and magnitude of the EMF.
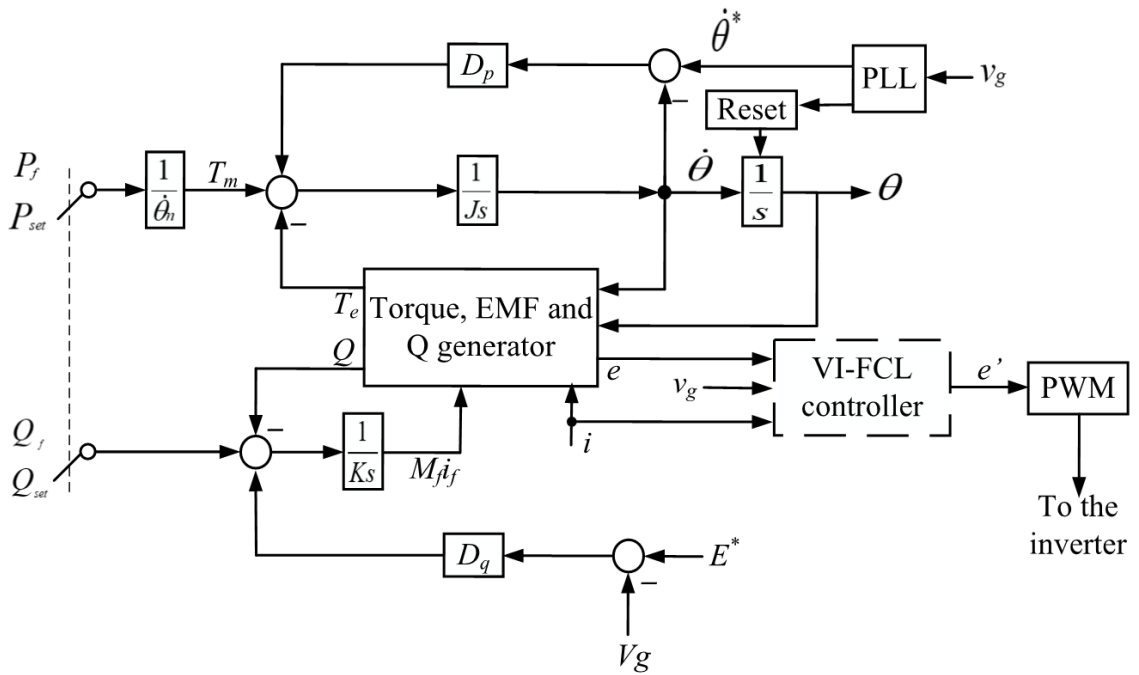
Figure 5.1. The proposed synchronverter controller.
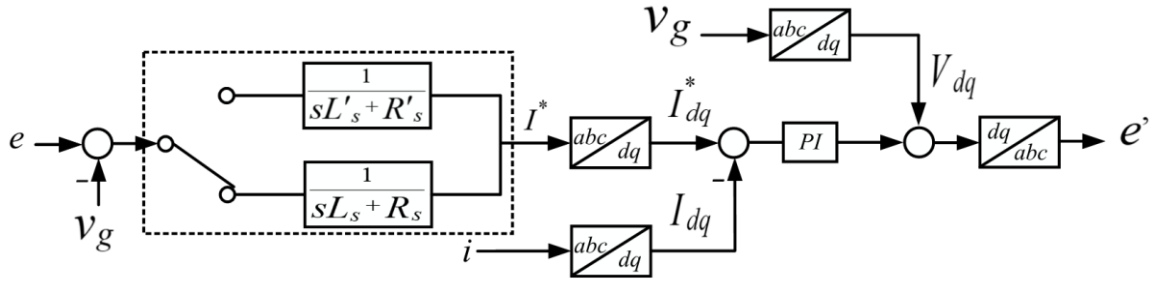
Figure 5.2. The proposed VI-FCL to limit the current during faults.

To demonstrate the effectiveness of the proposed VI-FCL, time-domain simulations are carried out using the grid-synchronverter test system. First, the current saturation is disabled, and R'_s and L'_s are assigned twice values of R_s and L_s during the fault. It is noteworthy that, R'_s and L'_s are active only during faulty conditions.
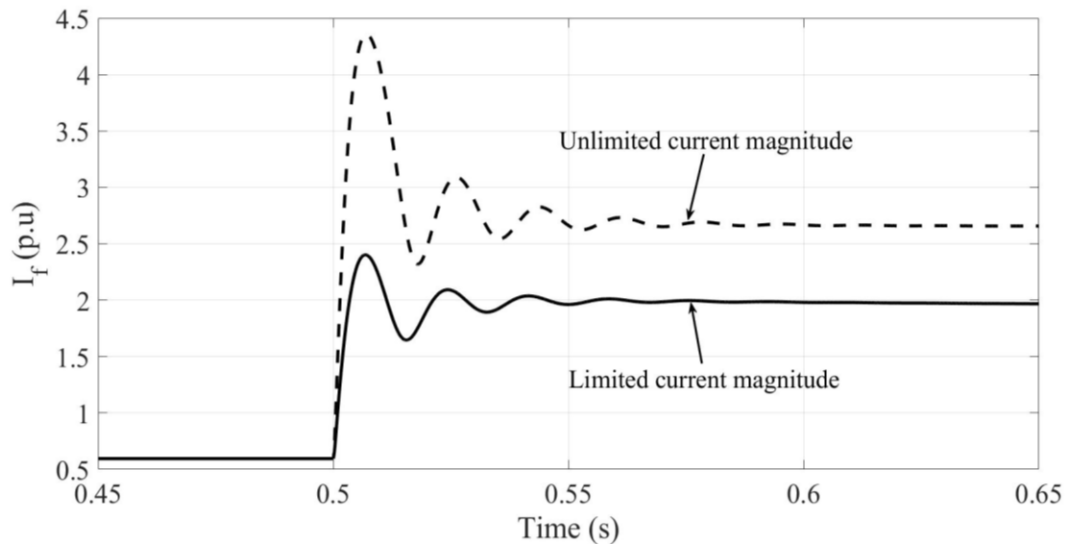
Figure 5.3. Synchronverter's fault currents with and without due to VI-FCL (prefault power setpoints).

Figure 5.3 depicts the fault currents of the synchronverter with and without the VI-FCL when the prefault power setpoints are enabled.
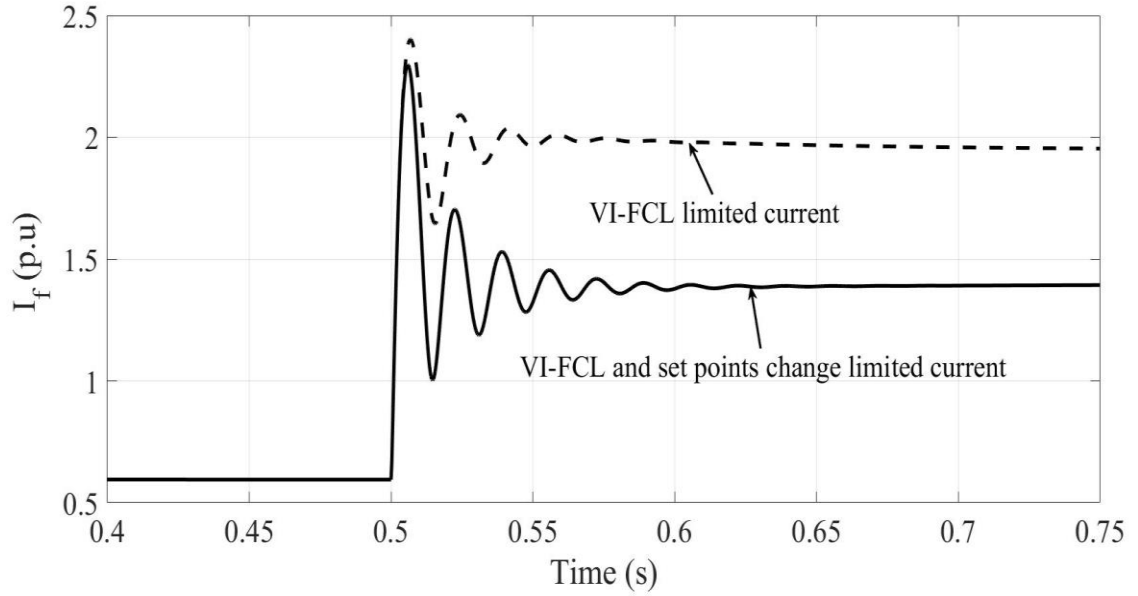
Figure 5.4. Synchronverter's fault currents with and without due to VI-FCL (proposed power setpoints).

The VI-FCL could reduce the fault current without the need for a hard limiter; however, the fault current is around 2.0 p.u. Next, the proposed setpoints for the real and reactive powers are enabled in conjunction with the VI-FCL. As shown in Figure 5.4, the inverter's current could be further limited to a value below 1.5 p.u. when the new real and reactive power setpoints are used during the fault. These results confirm the justification behind updating the real and reactive power setpoints along with enabling the VI-FCL. The optimal selection of the VI-FCL parameters is discussed and verified in the next section.

5.3 Proposed Two-Stage OPC

The VI-FCL controller proposed in the previous section has the benefits of limiting the current during faults and keep the voltage source model of the synchronverter intact, as shown in Figure 5.5.

39
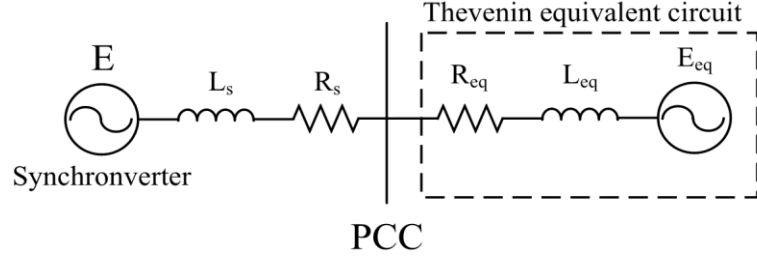
Figure 5.5. Synchronverter equivalent model.

In which, the grid is represented by an equivalent circuit, where E_{eq} is the grid equivalent voltage, R_{eq} is the grid equivalent resistance, and L_{eq} is the equivalent grid inductance. Thus, the synchronverter is modeled as a voltage source in the proposed two-stage optimization. The proposed two-stage OPC scheme guarantees feasibly and returns a solution at a much faster pace as opposed to solving the unified OPC program defined in Section 4.3. The proposed OPC imposes the constraints related to the VI-FCLs and the fault current magnitude in the first stage. The outcome of this stage is the fault currents and parameters of the VI-FCL that are required to perform the traditional OPC.

To calculate the fault current generated by a synchronverter subjected to a balanced fault, the algorithm suggested in [2] for short circuit current calculations is employed. The main concept in fault current calculation is to consider a short period of 0.2s. This short period is divided into smaller time segments. In each segment, the following sequence is applied:

(i)   Measuring the electromagnetic torque T_e, reactive power Q, synchronverter's EMF magnitude E, and synchronverter's angular frequency $\dot{\theta}$ are measured.

(ii)   Calculating the virtual acceleration and the rate of change in E using

$$\ddot{\theta} = \frac{1}{J}\left(Tm - Te - Dp\left(\dot{\theta}^* - \dot{\theta}\right)\right) \tag{5.4a}$$

$$\frac{dE}{dt} = \frac{d\dot{\theta}}{dt} + \frac{\dot{\theta}}{K}\left(\frac{d(M_f i_f)}{dt}\right) \tag{5.4b}$$

(iii)   Integrating (5.4a) to get $\Delta\dot{\theta}$, and integrating (5.4b) to get ΔE

(iv)   Updating the magnitude E and the frequency $\dot{\theta}$ by adding their values to the changes calculated in the previous step

$$E = E + \Delta E \tag{5.5a}$$

$$\dot{\theta} = \dot{\theta} + \Delta\dot{\theta} \tag{5.5b}$$

(v)   Calculating the values of the AC and DC components, i.e., the aperiodic component decaying with time and the periodic component. The fault current is the sum of both components as given by

$$i_{dc} = \left(\frac{E'_{eq}\sin(\theta'_2 - \gamma)}{\sqrt{R'^2 + (\omega L')^2}} - \frac{E_{eq}\sin(\theta_2 - \gamma)}{\sqrt{R^2 + (\omega L)^2}}\right)e^{-\frac{t}{Ta}} \tag{5.6a}$$

$$i_{ac} = \left(\frac{E\sin(\omega t + \theta - \gamma)}{\sqrt{R'^2 + (\omega L')^2}} - \frac{E'_{eq}\sin(\omega t + \theta'_2 - \gamma)}{\sqrt{R'^2 + (\omega L')^2}}\right) \tag{5.6b}$$

$$i_f = i_{dc} + i_{ac} \tag{5.6c}$$

where E_{eq} and θ_2 are the grid equivalent voltage amplitude and phase, respectively, during normal conditions. E'_{eq} and θ'_2 are the equivalent voltage magnitude and phase during the fault, respectively. R and L depend on the synchronverter internal impedance and the grid equivalent impedance as given by

$$R = R_s + R_{eq} \tag{5.7a}$$

$$L = L_s + L_{eq} \tag{5.7b}$$

During faults, R and L change to R' and L' to model the current limiting mechanism. Thus, R' and L' are defined as

$$R' = R_s' + R'_{eq} \tag{5.8a}$$

$$L' = L_s' + L'_{eq} \tag{5.8b}$$

where R_s' and L_s' are the synchronverter's resistance and impedance during faults, respectively. These parameters include the proposed VI-FCL components to limit the fault current to less than 1.5 p.u. as follows:

$$R_s' = R_s + R_{FCL} \tag{5.9a}$$

$$L_s' = L_s + L_{FCL} \tag{5.9b}$$

The impedance's angle γ and the time constant T_a are calculated by

$$\gamma = tan^{-1}\left(\frac{\omega L'}{R'}\right) \tag{5.10a}$$

$$T_a = \frac{L'}{R'} \tag{5.10b}$$

The described short-circuit current calculation method is the core of the first stage of the proposed two-stage OPC because it allows for imposing and modeling the VI-FCL constraints.

An overall flow chart describing the proposed two-stage OPC is shown in Figure 5.6. In the first stage, the magnitude of the periodic current component of each synchronverter is calculated by

$$I_f^{(d)} = \frac{(E - V'_{pcc})^{(d)}}{\sqrt{((R_s + R_{FCL})^{(d)})^2 + (\omega(L_s + L_{FCL})^{(d)})^2}} \tag{5.11}$$
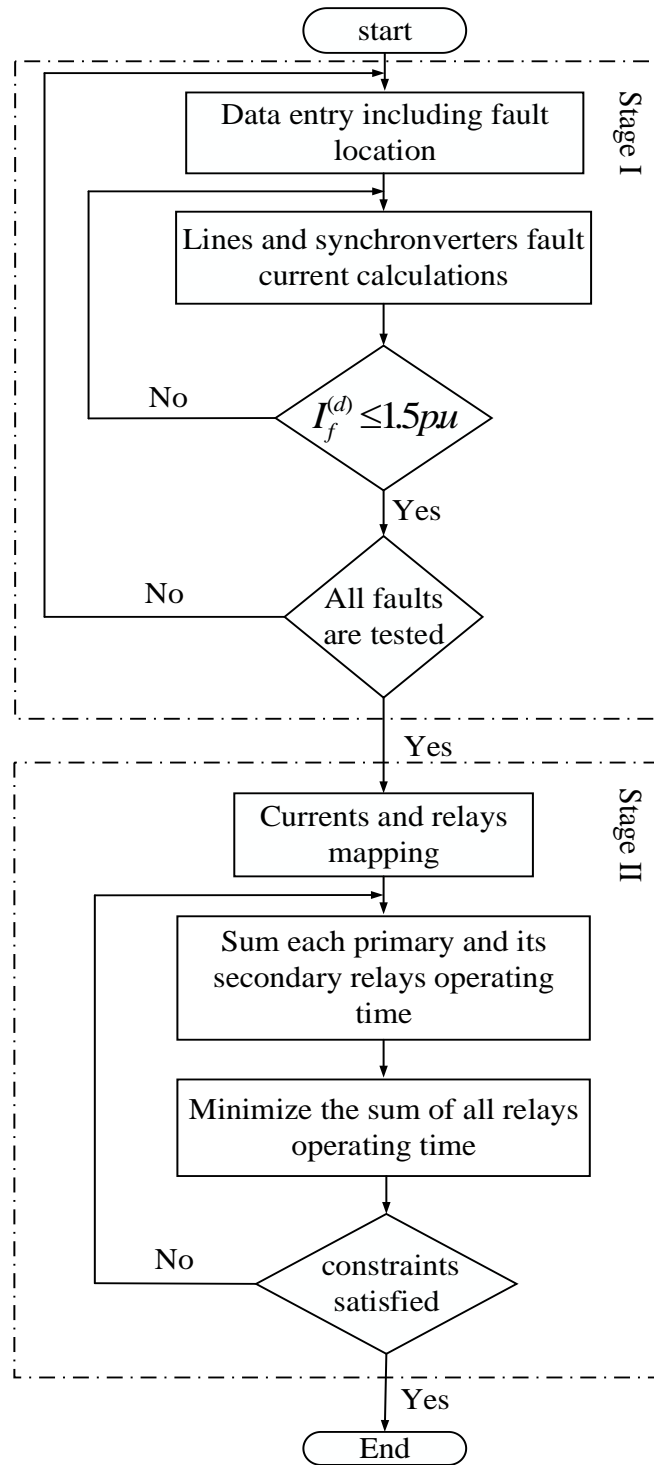
Figure 5.6. Proposed two-stage OPC flow chart.

The objective of the first stage is to minimize the summation of all fault currents injected by the synchronverters as

$$\text{Min } I = \sum_{d=1}^{D} I_f^{(d)} \tag{5.12}$$

The superscript d is the synchronverter identifier, while D is the total number of synchronverters in the ADN. The variables to be determined are the resistances and inductances of the VI-FCLs, i.e., $R_{FCL}^{(d)}$ and $L_{FCL}^{(d)}$. The reactance of a VI-FCL is set to be six times bigger than its resistance, which corresponds to an $X/R = 6$. Therefore, the following bounds on the VI-FCL resistance and inductance are imposed

$$R_{FCL_{min}}^{(d)} \leq R_{FCL}^{(d)} \leq R_{FCL_{max}}^{(d)} \qquad \forall d \tag{5.13a}$$

$$\frac{6R_{FCL_{min}}^{(d)}}{2\pi f} \leq L_{FCL}^{(d)} \leq \frac{6R_{FCL_{max}}^{(d)}}{2\pi f} \qquad \forall d \tag{5.13b}$$

A set of nonlinear constraints is imposed to limit the magnitude of the synchronverters fault current to a specific value as in (4.3). The returned results from the first stage are the fault currents flowing in each branch and the limited synchronverters fault currents along with the VI-FCLs' parameters.

The second stage of the proposed OPC scheme is a reformulation of the classic OPC program given by (3.16)–(3.19). The OPC formulation is simplified by moving the VI-FCL and current limits constraints to the first stage. Thus, the solver in the second stage determines only the optimal relays' settings.

5.4 Conclusion

This chapter explains the proposed VI-FCL control design for a synchronverter in ADNs. The proposed VI-FCL controller to limit the fault current from synchronverters is demonstrated. A two-stage OPC scheme is proposed to incorporate the synchronverter VI-FCLs in short-circuit current calculations. The first stage determines the parameters of the

VI-FCLs to limit the fault current of each synchronverter to a certain threshold as well as calculates the fault current through each line of the ADN. In the second stage, the OPC is formulated contingent upon the obtained VI-FCLs from the first stage. The two-stage OPC represents a cost-effective protection scheme to protect ADNs with synchronverters.

CHAPTER 6

PERFORMANCE EVALUATION OF THE PROPOSED SOLUTION

6.1 Introduction

In this chapter, the synchronverter model with VI-FCL is assessed and verified. The verification is done by comparing the results from the fault current calculations to the results from fault currents obtained by time-domain simulations. Further, the performance of the proposed two-stage OPC is tested on the Canadian 9-bus and IEEE 30-bus systems. The need for an adaptive VI-FCL formulation is justified to keep a detectable fault current regardless of the fault location. The proposed adaptive VI-FCL is also evaluated and validated. Furthermore, the proposed OPC is used to obtain the parameters of the adaptive VI-FCLs.

6.2 Proposed VI-FCL Evaluation and Validation

The proposed controller developed and tested for an arbitrary value of VI-FCL in the previous chapter. The evaluation is done in this section by using the resistance and inductance components that limit the fault current generation to less than 1.5 p.u. based on the output of the first stage. Figure 6.1 shows the current limitation when a synchronverter is subjected to a balanced bolted fault at its terminals. The proposed VI-FCL can successfully limit the fault current to a value of less than 1.5 p.u. in steady-state.
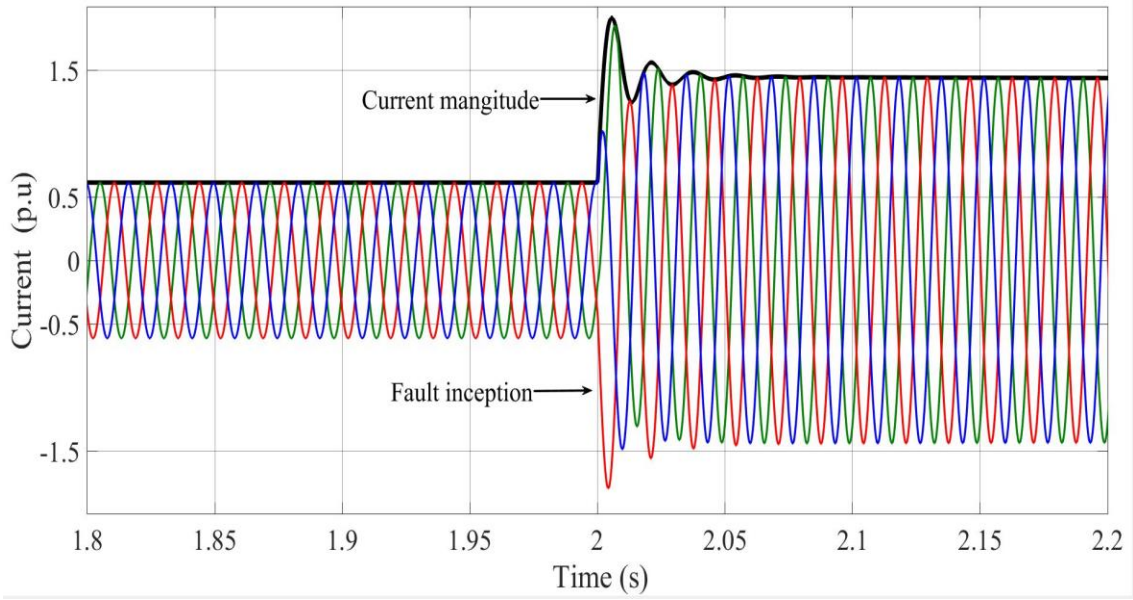
Figure 6.1. Limited synchronverter's fault current during a balanced fault.

The voltage source model used in the proposed two-stage OPC is verified in two steps. The first step is a simple system of an inverter controlled by the proposed VI-FCL controller and connected to a grid represented as a voltage source model, as shown in Figure 3.3. The values of the synchronverter parameters used in this simulation are shown in Table 3.1. The first test of validation is done by simulating the generated fault current if the grid voltage drops from its nominal down to 0 p.u. Figure 6.2 shows the calculated fault currents versus the simulated fault currents during the voltage drop.
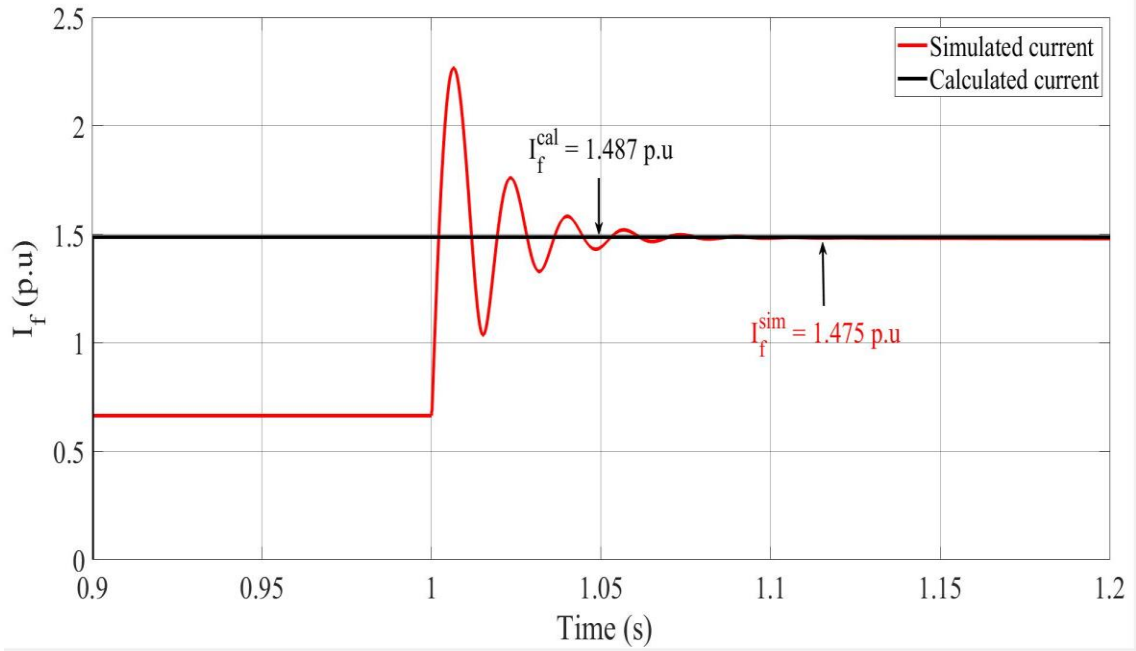
Figure 6.2. Synchronverter simulated current compared to the calculated current for the first case.

As seen in Figure 6.2, the calculated current is 1.487 p.u., and the simulated current is 1.475p.u. resulting in a deviation less than 0.5 %.
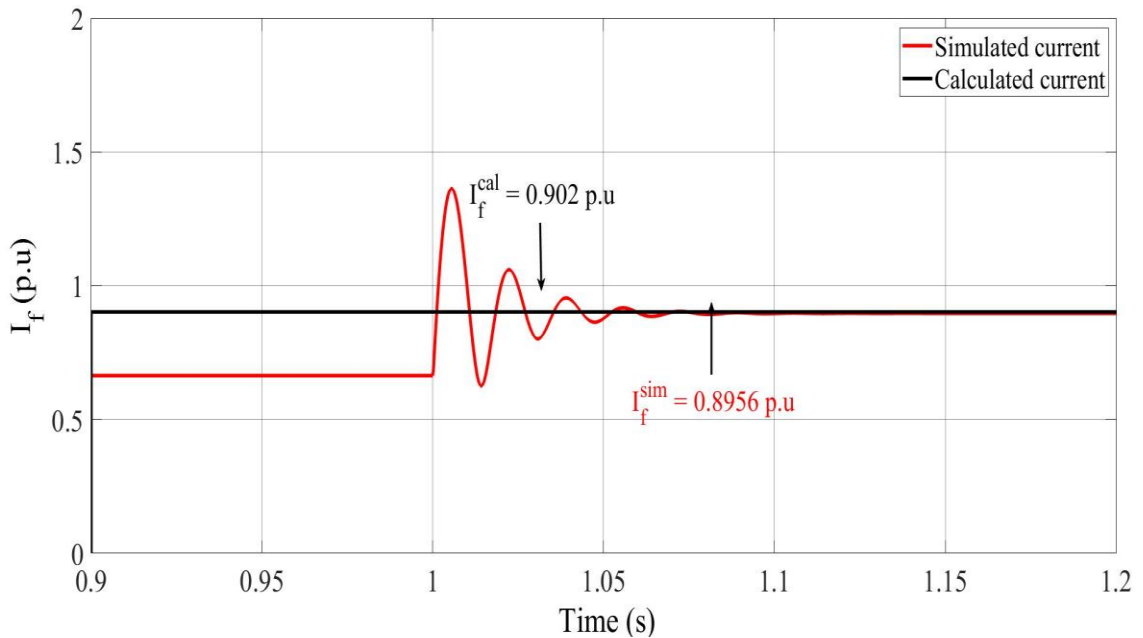
Figure 6.3. Synchronverter Simulated current compared to the calculated current for the second case.

Second, the short-circuit current calculation is assessed for a less severe fault that causes the terminal's voltage to drop to 0.4 p.u. As shown in Figure 6.3, the simulated current has a magnitude of 0.8954 p.u., which almost matches the calculated current (i.e., 0.902 p.u.). the deviation in this case is less than 1%.
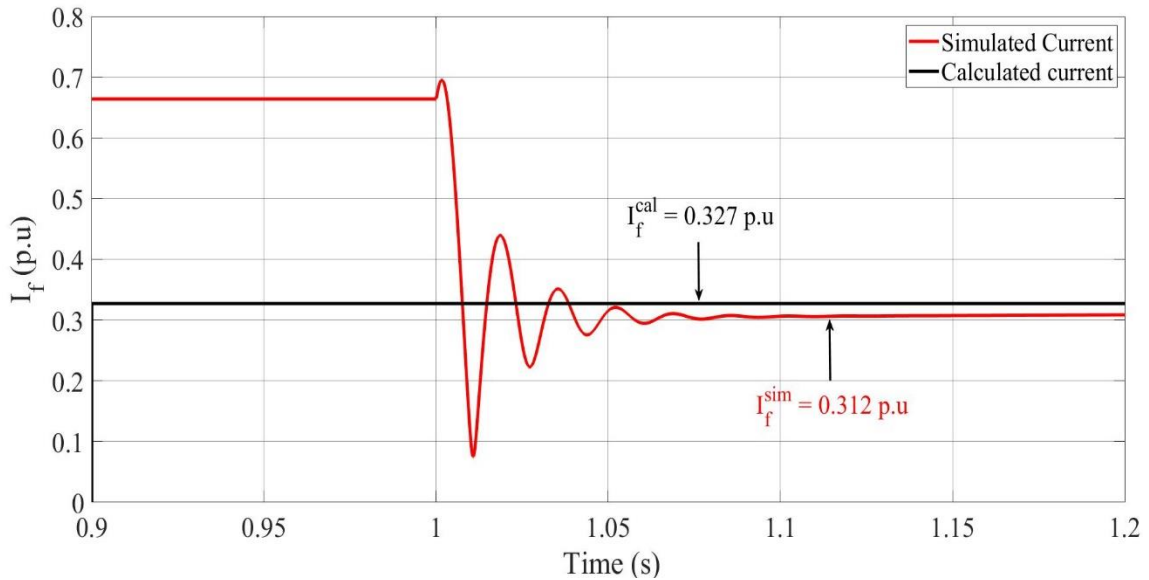
Figure 6.4. Synchronverter Simulated current compared to the calculated current for the third case.

The third validation case study simulates a fault that results in a voltage drop to 0.2 p.u. Under this condition, the simulated current is 0.327 p.u., while the calculated current is 0.312 p.u. as magnitudes, as shown in Figure 6.4. The compared current magnitudes are in match with a deviation of 4.45 %.

The second step of the validation is done by simulating faults in the 9-bus system shown in Figure 3.9. Each synchronverter is subjected to faults at its terminal. Synchronverter denoted DG1 at bus 4 is tested for three faults located at bus 4, synchronverter denoted DG2 at bus 5 is tested for three faults located at bus 5, synchronverter denoted as DG 3 at bus 6 is tested for three faults located at bus 6 and synchronverter denoted as DG4 at bus 9 is tested for three faults located at bus 9.

Table 6.1 shows the comparison between the simulated and calculated currents. In all three faults, the deviation is less than 5%. These results confirm the accuracy of the VI-FCL modeling in short-circuit calculations.

Table 6.1. Synchronverter model validation for 9-bus system.

DG 1 calculated and simulated results comparison			
R_f $(p.u.)$	$I_{cal}^{(1)}$ $(p.u.)$	$I_{sim}^{(1)}(p.u.)$	Dev %
0	0.744	0.724	2.19
0.09	0.456	0.447	1.95
0.35	0.199	0.201	1.04
DG 2 calculated and simulated results comparison			
R_f $(p.u.)$	$I_{cal}^{(2)}$ $(p.u.)$	$I_{sim}^{(2)}(p.u.)$	Dev %
0	0.745	0.732	1.75
0.09	0.456	0.445	2.50
0.35	0.200	0.202	0.99
DG 3 calculated and simulated results comparison			
R_f $(p.u.)$	$I_{cal}^{(3)}$ $(p.u.)$	$I_{sim}^{(3)}(p.u.)$	Dev %
0	0.749	0.724	3.24
0.09	0.465	0.450	3.22
0.35	0.199	0.200	0.50
DG 4 calculated and simulated results comparison			
R_f $(p.u.)$	$I_{cal}^{(4)}$ $(p.u.)$	$I_{sim}^{(4)}(p.u.)$	Dev %
0	0.7440	0.7120	4.22
0.09	0.4562	0.4431	2.87
0.35	0.1998	0.2010	0.99

It is worth noting that the displayed results in Table 6.1 are calculated according to 8 MVA base power and 480V/12.47 kV base voltages. Thus, the maximum fault current is 0.75 p.u. which corresponds to 1.5 p.u. when the synchronverter ratings are used as the system bases.

The developed VI-FCL model kept the synchronverter model intact because the inverter's current is limited by an impedance, not a hard limiter.

6.3 Proposed Two-Stage OPC Performance Evaluation

The outcomes of the proposed two-stage OPC schemes are examined. The values of VI-FCL components to limit the fault currents, and the relays optimal settings are

determined. The system under study is the same 9-bus system. The results obtained are the resistive and inductive components of each VI-FCL, and relays operating time corresponding to the determined relays optimal settings. The calculations are based on 8 MVA and 480V/12.47kV bases. Table 6.2 shows the output of the first stage, i.e., the required VI-FCL resistances and inductances to limit the fault current at all possible locations.

Table 6.2. VI-FCL components of each synchronverter of the 9-bus system.

Synchronverter location	$R_{FCL}^{(d)}$ $(p.u.)$	$L_{FCL}^{(d)}$ $(p.u.)$
Bus 4	0.184	0.00293
Bus 5	0.183	0.00291
Bus 6	0.184	0.00293
Bus 9	0.182	0.00289

The shown values of the VI-FCLs are obtained for the worst-case scenario, which is a bolted fault at the synchronverter's terminal. Utilizing the VI-FCL parameters, the second stage of the proposed OPC scheme is conducted to determine the optimal relays' settings, as displayed in Table 6.3. Then, the obtained relay settings are used to calculate the operating times as shown in Table 6.4

Table 6.3. Relays optimal settings of the 9-bus system.

Relay	$TDS(s)$	I_p $(p.u.)$	Relay	$TDS(s)$	I_p $(p.u.)$
1	0.1392	1.2501	12	0.1290	1.3905
2	0.1504	1.2500	13	0.0557	1.2500
3	0.0914	1.2500	14	0.1590	1.2500
4	0.1950	1.2501	15	0.0101	1.2501
5	0.0466	1.2673	16	0.1908	0.6250
6	0.2439	1.2500	17	0.2850	0.6250
7	0.0101	1.2500	18	0.0265	0.6250
8	0.1828	1.2500	19	0.0282	0.6251
9	0.1229	1.2501	20	0.0210	0.6252
10	0.1757	1.2501	21	0.0293	1.3905
11	0.1128	1.2500			

Table 6.4. Relays' operating times corresponding to the optimal relays' settings.

Fault	P_1	B_{11}	B_{12}	P_2	B_{21}	B_{22}
F10	R1	R10	R17	R2	R4	
	0.5126	0.7121	0.7119	0.6324	0.8319	
F11	R3	R1		R4	R6	
	0.3675	0.5667		0.7551	0.9546	
F12	R5	R3		R6	R8	R18
	0.2047	0.4040		0.8606	1.0597	1.0608
F13	R7	R5	R18	R8	R19	
	0.0339	0.233	1.0608	0.9304	1.1298	
F14	R9	R2	R17	R10	R12	R20
	0.5008	0. 6998	0.7119	0.6385	0.8378	0.8416
F15	R11	R9	R20	R12	R14	
	0.3707	0.5700	0.8416	0.7334	0.9329	
F16	R13	R11		R14	R16	
	0.2147	0.4138		0.8579	1.0574	
F17	R15	R13		R16	R21	
	0.0400	0.2391		0.9710	1.1722	
T = 25.6676 s						

The difference in operating time between any backup relay and its primary relay is equal or greater than 0.2 s, which indicates the *CTI* constraints are satisfied, conforms effective coordination.

The proposed two-stage OPC may not converge to a feasible solution if the fault resistance is not low enough. The VI-FCL is sized according to the worst-case condition, which could be too conservative. Therefore, the need for an adaptive VI-F that varies according to the fault condition arises. The following section states the problem that could appear due to the use of fixed VI-FCLs and proposes a remedy for it.

6.4 Adaptive VI-FCL Problem Statement and Evaluation

Referring to (3.17), let's consider R19, which is associated with the synchronverter connected at bus 5. This relay acts as a backup for R8. Figure 6.5 shows the layout of the section under investigation.
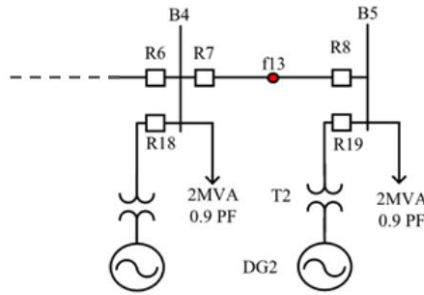
Figure 6.5. schematic diagram of the section under investigation.

If the fault resistance during f13 fault inception is not around zero, the calculated VI-FCL may be larger than needed to limit the fault current. Thus, the fault current could be limited to a value less than the relay's pickup current. Consequently, the resultant operating time is an infinite or negative number, as shown in Table 6.5. Thus, GA returns an infeasible solution. Theoretically, a solution could be available by relaxing the fault current limit. As a demonstration, the proposed two-stage OPC is performed to consider three different fault resistances (0 Ω, 0.5 Ω, and 2 Ω.) The values of the relays' optimal settings are global for all the resistances listed in Table 6.6

Table 6.5. R19 operating times corresponding to different fault currents.

R_f (Ω)	$I_f^{(2)}$ ($p.u.$)	t_{R19} ($seconds$)
0	0.745	1.047
1	0.456	-0.5814
5	0.200	-0.1622

Table 6.6. Relays global optimal settings for different fault resistances.

Relay	$TDS(s)$	I_p (p.u.)	Relay	$TDS(s)$	I_p (p.u.)
1	0.1266	1.4355	12	0.1269	1.2507
2	0.1500	1.2500	13	0.0595	1.2500
3	0.0809	1.4895	14	0.1570	1.2500
4	0.1945	1.2500	15	0.0100	1.2500
5	0.0465	1.2705	16	0.1848	1.2830
6	0.2432	1.2500	17	0.2656	0.7261
7	0.0100	1.2500	18	0.2396	0.6250
8	0.1825	1.2501	19	0.2536	0.6251
9	0.1224	1.2500	20	0.1868	0.6251
10	0.1606	1.4151	21	0.2570	0.6250
11	0.1022	1.4941	T = 90.2 s		

However, this solution is impractical since a relaxation on the VI-FCL leads to fault currents higher than 2.5 p.u., and this would damage the inverter's switches. An adaptive impedance is proposed to keep the synchronverter protected and ensure detectable fault currents, which will make the proposed two-stage OPC program feasible to solve.

The proposed adaptive VI-FCL depends on the value of the constant VI-FCL formulated earlier to intercept bolted balanced faults. The adaptive VI-FCL controller varies the value of the VI-FCL components according to the synchronverter's terminal voltage. If the fault is bolted, the full value of the fixed VI-FCL impedance will be engaged. When faults are less severe—which corresponds to relatively lower voltage drops—only partial engagement of the fixed VI-FCL is allowed. The adaptive VI-FCL represents a droop characteristic in terms of the magnitude of the inverter's terminal voltage as follows:

$$Z_{adp} = mV_t + b \tag{6.1}$$

where Z_{adp} is the magnitude of the adaptive impedance, m is the slope of the line representing the adaptive impedance, and b is a constant. The slope of the adaptive impedance line is determined based on

$$m = -\left(\frac{Z_{adp}^{max} - Z_{adp}^{min}}{V_t^{max} - V_t^{min}}\right) \qquad (6.2)$$

where Z_{adp}^{max} is the maximum value of the adaptive VI-FCL, which corresponds to the fixed

value of the VI-FCL imported from the first stage of the proposed OPC scheme, Z_{adp}^{min} is

the minimum magnitude of the adaptive VI-FCL to be engaged when the voltage drop is

minimal, V_t^{max} and V_t^{min} denotes the maximum and minimum values of V_t. The value of

b can be calculated as follows:

$$b = Z_{adp}^{max} - mV_t^{min} \qquad (6.3)$$

This formulation is done to keep the fault current generated from a synchronverter

during low-impedance faults detectable. Finally, the values of the adaptive VI-FCL

components are calculated according to the following equations

$$R_{adp} = \frac{Z_{adp}}{\sqrt{1 + (X/R)^2}} \qquad (6.4)$$

$$L_{adp} = \left(R_{adp}(X/R)\right)/2\pi f \qquad (6.5)$$

where X/R is equaled to 6.0, and f is the grid frequency. The proposed adaptive

formulation is tested to guarantee the current limitation and feasibility of the OPC program.

The synchronverter understudy is DG2. Table 6.7 displays the parameter of the adaptive

VI-FCL used in this case study.

Table 6.7. Parameters of the adaptive VI-FCL for the synchronverter at bus 5.

Parameter	Value
Z_{adp}^{max}	1.1156 p.u.
Z_{adp}^{min}	0.2688 p.u.
V_t^{max}	0.8 p.u.
V_t^{min}	0 p.u.

The value of the maximum adaptive VI-FCL is imported from the first stage of the proposed two-stage OPC; the minimum value is calculated based on

$$Z_{adp}^{min} = \frac{E - V_t^{max}}{I_{f_{max}}^{(2)}}$$
(6.6)

Figure 6.6 shows the droop characteristic representing the adaptive VI-FCL. The proposed adaptive VI-FCL is tested using time-domain simulations to verify its performance. Figure 6.7 demonstrates the operation of the adaptive VI-FCL at different voltage drops. The proposed adaptive VI-FCL ensures a detectable level of fault current at various voltage drops.
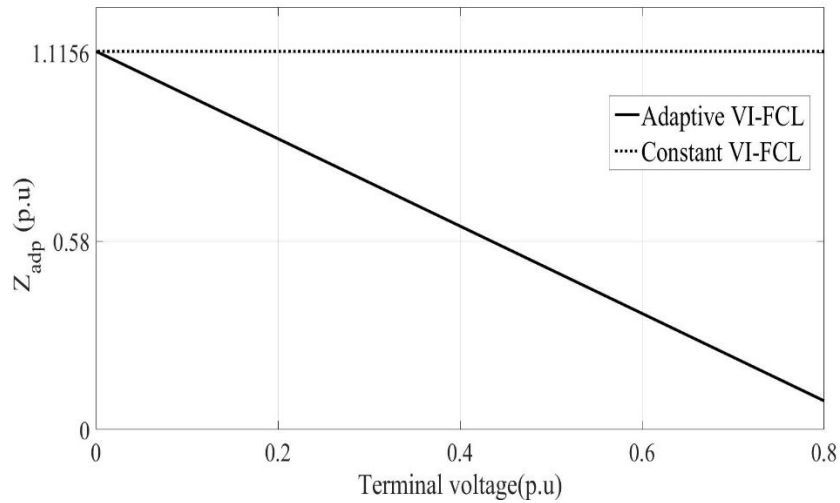
Figure 6.6. Calculated adaptive VI-FCL compared to constant VI-FCL.
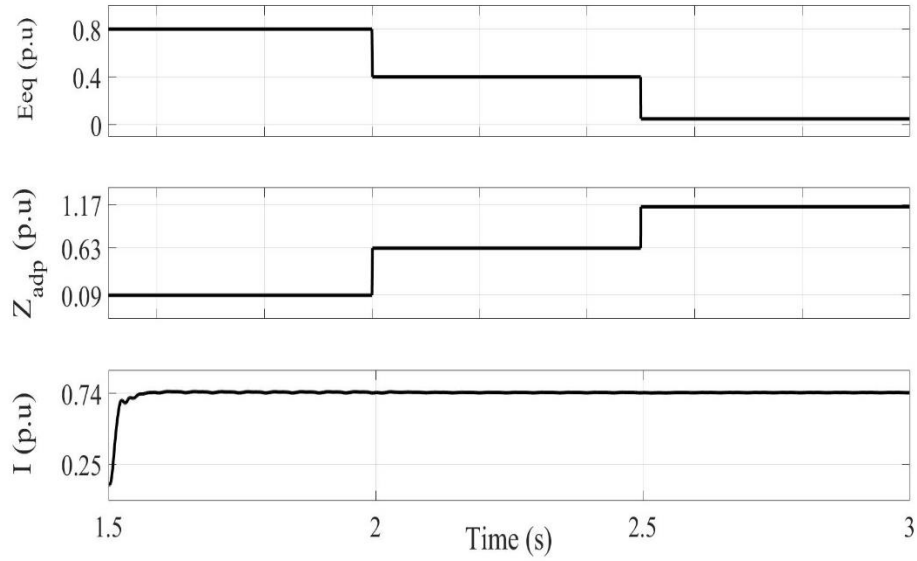
Figure 6.7. Simulated adaptive VI-FCL to keep the constant current during voltage change.

As this case applies to R19, the relay measures a high fault current, and as a result, it responses quickly. In other words, the adaptive VI-FCL ensures a margin between the relay's measured current and its pickup value. The parameters for all adaptive VI-FCLs are listed in Table 6.8.

Table 6.8. Parameters of all adaptive VI-FCLs.

Synchronverter location	m	b
Bus 4	-1.0633	1.1192
Bus 5	-1.0585	1.1156
Bus 6	-1.0645	1.1204
Bus 9	-1.0494	1.1083

6.5 Case Study on the IEEE 30-bus System

In this section, the calculations are applied to a bigger system to assert the effectiveness of the proposed two-stage OPC scheme.

The system under study is the distribution portion of the IEEE 30-bus system, which is displayed in Figure 6.8. and its data is available in [52]. Synchronverters are connected at various locations. Each synchronverter is rated at 10 MVA and connected through a 480 V/33 kV step transformer. Buses 2,8 and 12 are the feeding nodes from the main grid through three 50 MVA, 132 kV/33 kV. The network is equipped with 56 relays. The bolted balanced fault locations are the midpoint of each line. The synchronverters are subjected to bolted faults at their terminals, similar to the previous study. These faults are used to calculate the required VI-FCL to limit the fault current.

The proposed two-stage OPC is applied to determine the parameters of VI-FCLs and the relays' optimal settings. Table 6.9 displays the parameters of the fixed VI-FCLs calculated in the first stage of the proposed OPC.
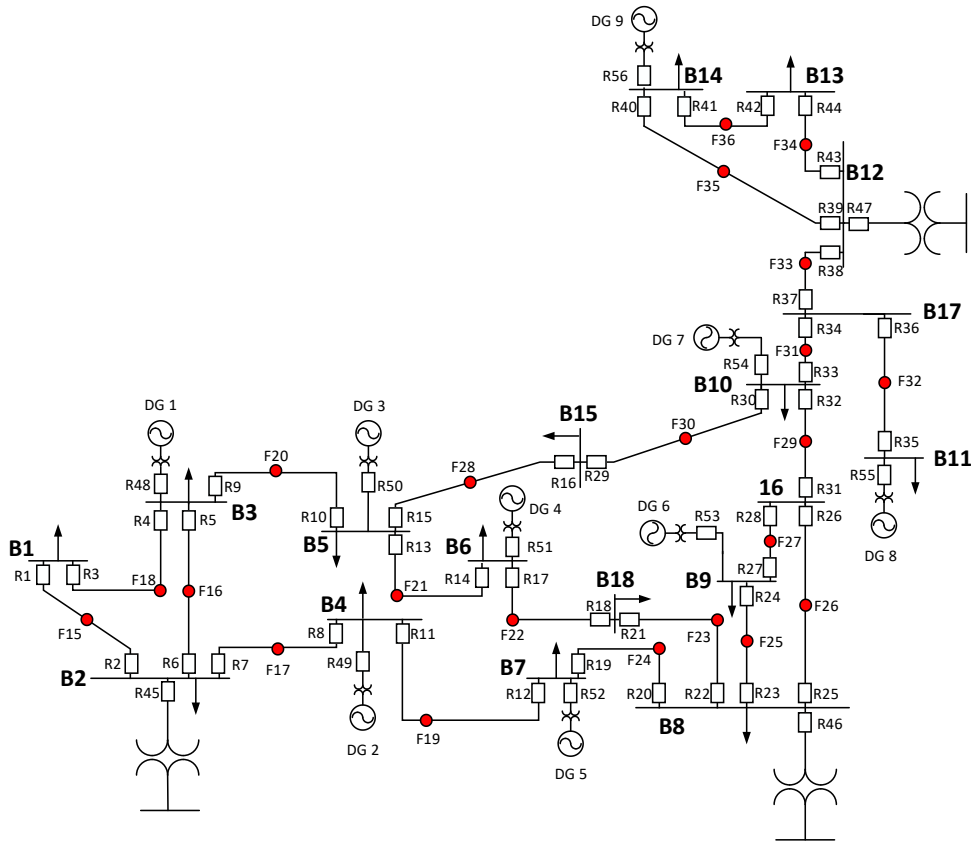
Figure 6.8. Distribution network of the IEEE 30-bus system.

Table 6.9. Parameters of fixed VI-FCLs used with the IEEE 30.-bus system.

Synchronverter location	$R_{FCL}^{(d)}$ (p.u.)	$L_{FCL}^{(d)}$ (p.u.)
Bus 3	0.0539	0.0008585
Bus 4	0.0537	0.0008548
Bus 5	0.0540	0.0008601
Bus 6	0.0537	0.0008545
Bus 7	0.0539	0.0008573
Bus 9	0.0537	0.0008554
Bus 10	0.0540	0.0008601
Bus 11	0.0528	0.0008405
Bus 14	0.0531	0.0008456

The relays' optimal settings are determined in the second stage and listed in Table 6.10. These settings result in the relays' operating times shown in Table 6.11. As can be seen, the protection coordination is maintained, i.e., CTI is equal to 0.2s or higher. Also, the inverters' currents are limited to the current magnitudes to less than 1.5 p.u. These results confirm the successful operation of the proposed two-stage OPC.

Table 6.10. Relays' optimal settings in IEEE 30-bus system.

Relay	$TDS(s)$	I_p $(p.u)$	Relay	$TDS(s)$	I_p $(p.u)$
1	0.0501	1.2501	29	0.0907	1.2500
2	0.0986	1.2501	30	0.1331	1.2500
3	0.0598	1.2501	31	0.1123	1.2500
4	0.0853	1.2500	32	0.1097	1.2500
5	0.0950	1.2501	33	0.1226	1.2501
6	0.1143	1.2500	34	0.1097	1.2500
7	0.1588	1.2500	35	0.0573	1.2501
8	0.1047	1.2501	36	0.0501	1.2500
9	0.1216	1.2500	37	0.0914	1.2894
10	0.1145	1.2501	38	0.1328	1.2500
11	0.1385	1.2634	39	0.0907	1.2500
12	0.1267	1.2501	40	0.0500	1.2500
13	0.1087	1.2500	41	0.0846	1.2503
14	0.0963	1.2501	42	0.0501	1.2500
15	0.1332	1.2507	43	0.0855	1.2614
16	0.0894	1.2500	44	0.0689	1.2500
17	0.0823	1.2526	45	0.0500	1.2500
18	0.1044	1.2500	46	0.0500	1.2500
19	0.1318	1.2500	47	0.0500	1.2500
20	0.1580	1.2501	48	0.0500	1.2500
21	0.0677	1.2525	49	0.0501	1.2500
22	0.1541	1.2505	50	0.0501	1.2500
23	0.1098	1.2500	51	0.0500	1.2500
24	0.0647	1.2501	52	0.0500	1.2500
25	0.1260	1.2500	53	0.0500	1.2500
26	0.0815	1.2500	54	0.2607	1.2501
27	0.0924	1.2500	55	0.2638	1.2500
28	0.0722	1.2500	56	0.2335	1.2528

Table 6.11. Relays operating time for IEEE 30-bus system.

FL	P_1	B_{11}	B_{12}	B_{13}	B_{14}	P_2	B_{21}	B_{22}	B_{23}	B_{24}
15	R1	R4				R2	R5	R8	R45	
	0.237	0.437				0.2968	4.729	0.62	1.984	
16	R5	R3	R10	R48		R6	R1	R8	R45	
	0.329	0.723	0.533	1.999		0.3602	0.817	0.6	1.984	
17	R7	R5	R1	R45		R8	R12	R49		
	0.483	0.684	0.914	1.984		0.3811	0.607	2.002		
18	R3	R2				R4	R6	R10	R48	
	0.266	0.467				0.2714	0.933	0.557	1.998	
19	R11	R7	R49			R12	R20	R52		
	0.484	0.688	2.004			0.4299	0.652	1.995		
20	R9	R6	R3	R48		R10	R14	R16	R50	
	0.408	0.606	0.604	1.994		0.3716	0.582	0.571	1.994	
21	R13	R16	R9	R50		R14	R18	R51		
	0.343	0.612	0.616	1.994		0.3692	0.568	1.990		
22	R17	R13	R51			R18	R22			
	0.292	0.493	1.990			0.3951	0.605			
23	R21	R17				R22	R19	R24	R26	R46
	0.192	0.395				0.6896	0.89	0.892	0.891	1.976
24	R19	R11	R52			R20	R21	R24	R26	R46
	0.485	0.685	1.995			0.4531	0.655	0.805	0.784	1.979
25	R23	R21	R19	R26	R46	R24	R28	R53		
	0.318	0.621	0.830	1.225	1.979	0.2624	0.462	1.978		
26	R25	R24	R21	R19	R46	R26	R32	R27		
	0.369	1.794	0.642	0.822	1.979	0.2997	0.499	0.986		
27	R27	R23	R53			R28	R25	R32		
	0.341	0.542	1.979			0.2421	0.713	0.515		

28	R15	R14	R9	R50	R16	R30		
	0.417	0.618	0.617	1.994	0.3617	0.565		
29	R31	R25	R27		R32	R34	R29	R54
	0.385	0.584	0.584		0.3526	0.600	0.622	0.619
30	R29	R15			R30	R31	R34	R54
	0.367	0.567			0.4151	0.621	0.617	0.619
31	R33	R31	R29	R54	R34	R35	R38	
	0.387	0.587	0.587	0.618	0.4036	0.605	0.604	
32	R35	R55			R36	R33	R38	
	0.381	0.616			0.1601	0.567	0.652	
33	R37	R33	R35		R38	R40	R44	R47
	0.333	0.533	0.617		0.4426	1.048	0.642	1.991
34	R43	R40	R37	R47	R44	R41		
	0.273	0.718	0.503	1.991	0.4334	0.635		
35	R39	R37	R44	R47	R40	R42	R56	
	0.294	0.495	0.623	1.991	0.2503	1.431	0.538	
36	R41	R39	R56		R42	R43		
	0.334	0.533	0.538		0.2349	0.434		
T = 119.57								

The need for adaptive impedance arises if different fault resistances are involved. As similar to the 9-bus system, the adaptive impedance is formulated to keep the synchronverters' current generation around the desired level. The test is done for three different fault resistances 0 ohms, 0.5 Ω, and 2 Ω. The values of fixed resistances and inductances listed in Table 6.9 are used to obtain the droop characteristics of the adaptive VI-FCLs, as given in Table 6.12.

Table 6.12. Parameters of adaptive VI-FCLs used with the IEEE 30.-bus system.

Synchronverter location	m	b
Bus 3	-0.1342	0.3279
Bus 4	-0.1341	0.3266
Bus 5	-0.1343	0.3285
Bus 6	-0.1343	0.3266
Bus 7	-0.1343	0.3279
Bus 9	-0.1342	0.3266
Bus 10	-0.1342	0.3285
Bus 11	-0.1343	0.3212
Bus 14	-0.1341	0.3230

The obtained relays' settings based on the adaptive VI-FCLs are listed in Table 6.13. These values maintain proper coordination between the DOCRs. For instance, as demonstrated in Table 6.14, the time difference between primary and back-up relays during f1–f5 is more than or equal to the CTI for the different fault resistances. Also, it is worthy noted that the operating times of R48 and R49 relays associated with synchronverters involved in Table 6.14 are maintained for all the fault resistances due to the adaptive VI-FCL that maintain the synchronverter's current higher than the associated relay's pickup current regardless of the fault location.

Table 6.13. Relays' global settings in IEEE 30-bus system.

Relay	$TDS(s)$	$I_p\ (p.u.)$	Relay	$TDS(s)$	$I_p\ (p.u.)$
1	0.1009	1.2500	29	0.1225	1.2506
2	0.1486	1.2515	30	0.1846	1.2503
3	0.1032	1.3440	31	0.1739	1.2884
4	0.1577	1.2512	32	0.1977	1.2577
5	0.1083	1.2502	33	0.1438	1.2500
6	0.1672	1.2500	34	0.1524	1.2562
7	0.1866	1.2905	35	0.1273	1.2582
8	0.1293	1.2506	36	0.0500	1.2502
9	0.1583	1.2587	37	0.1180	1.2570
10	0.1448	1.2505	38	0.1660	1.2665
11	0.1789	1.2500	39	0.1218	1.2500
12	0.1532	1.2500	40	0.0968	1.2560
13	0.1275	1.2520	41	0.1198	1.2543
14	0.1107	1.2754	42	0.1053	1.2504
15	0.1674	1.2521	43	0.1374	1.2533
16	0.1073	1.2500	44	0.0898	1.2501
17	0.1061	1.2574	45	0.2559	1.2500
18	0.1134	1.2776	46	0.4097	1.2666
19	0.1841	1.2503	47	0.4398	1.2501
20	0.1871	1.2516	48	0.0500	1.2500
21	0.1092	1.2688	49	0.0501	1.2500
22	0.1617	1.2500	50	0.0500	1.2500
23	0.1572	1.2504	51	0.0500	1.2500
24	0.1540	1.3565	52	0.0501	1.2500
25	0.1623	1.4569	53	0.0500	1.2500
26	0.1910	1.2508	54	0.0500	1.2500
27	0.1559	1.2532	55	0.0642	1.2533
28	0.1251	1.4366	56	0.0500	1.2500
T = 690.8690 s					

Table 6.14. Relays' operating times for different fault resistances.

FL	$R_f(\Omega)$	P$_1$	B$_{11}$	B$_{12}$	B$_{13}$	B$_{14}$	P$_2$	B$_{21}$	B$_{22}$	B$_{23}$
15	0	R1 0.4473	R4 0.8057				R2 0.4475	R5 0.818	R8 0.7659	R45 0.7804
16	0	R5 0.3749	R3 1.4278	R10 0.6734	R48 1.9838		R6 0.4709	R1 1.6454	R8 0.7414	R45 0.7804
17	0	R7 0.5759	R5 0.78	R1 1.8401	R45 0.7804		R8 0.4709	R12 0.7333	R49 1.9826	
15	0.5	R1 0.5425	R4 0.9282				R2 0.4853	R5 0.9729	R8 0.9009	R45 1.2268
16	0.5	R5 0.4189	R3 1.6298	R10 0.7828	R48 1.9838		R6 0.5831	R1 1.8211	R8 0.8948	R45 1.2268
17	0.5	R7 0.6351	R5 0.99	R1 3.9231	R45 1.2268		R8 0.5287	R12 0.8551	R49 1.9826	
15	2	R1 1.087	R4 2.0504				R2 0.7028	R5 1.4059	R8 2.5410	R45 1.4837
16	2	R5 0.7016	R3 2.5129	R10 1.2085	R48 1.9838		R6 0.9180	R1 2.4462	R8 3.0859	R45 1.4837
17	2	R7 0.8979	R5 2.1590	R1 1.2085	R45 1.4837		R8 0.9180	R12 2.4462	R49 1.9826	

6.6 Conclusion

In this chapter, the capability of VI-FCLs to limit the fault current is validated using a Canadian 9-bus distribution system. The proposed VI-FCL model and controller are validated by comparing short-circuit current calculations to fault currents obtained from time-domain simulations. Further, the proposed two-stage OPC is tested when adopting fixed VI-FCLs on the 9-bus system. It is observed that using fixed VI-FCLs could make the proposed OPC program infeasible when the fault resistance is not near zero. Therefore, adaptive VI-FCLs are proposed and implemented to adapt to different fault conditions. Simulation results prove the effectiveness of the proposed VI-FCLs in enhancing the

solution and avoiding unmet constraints since VI-FCLs ensure detectable faults currents even at relatively high fault resistance. Furthermore, the performance evaluation is conducted on the IEEE 30-bus system. As seen from the obtained results, the OPC solution is feasible and obtained at a low computational burden. The results presented in this chapter confirm that the proposed two-stage OPC scheme with adaptive VI-FCLs is a cost-effective strategy to protect ADNs powered with synchronverters.

CHAPTER 7

THESIS CONCLUSION AND FUTURE WORK

7.1 Thesis Conclusion

A survey is conducted to review topics related to ADNs, synchronverters, fault current limitations, and OPC, and to highlight the shortcomings addressed by the research presented in this thesis. The survey is followed by explaining the basics of synchronverter modeling and control and formulating the traditional OPC program. Then, the problem of inrush current from synchronverters is illustrated. The need for a voltage source model using VI-FCLs for OPC studies is stated. The problem statement is supported by simulation results. To address this problem, the traditional OPC is augmented by VI-FCLs to be solved in a unified manner; however, infeasibility issues could occur, which may require constraints relaxing.

Alternatively, a two-stage OPC scheme is proposed and formulated to handle the VI-FCL constraints separately from those for the relays' settings. The proposed scheme simplifies the OPC formulation and avoids infeasibility issues. Simulation results on the Canadian 9-bus system prove the successful operation of the proposed scheme when the fault resistance is near zero. However, infeasibility issue could occur when the fault resistance is relatively high. This problem occurs because fixed VI-FCLs may result in fault currents that are below the relays' pickup currents. To solve this issue, adaptive VI-FCLs are proposed to ensure a measurable margin between the fault current and the relay's pickup current. The proposed adaptive VI-FCL adopts a droop characteristic between the magnitude of the virtual impedance and the magnitude of the inverter's terminal voltage. Simulation results using the 9-bus and the IEEE 30-bus systems confirm the effectiveness

of the proposed two-stage OPC with adaptive VI-FCLs as cost-effective protection means of ADNs with synchronverters.

7.2 Future Work

Further research on the OPC of ADNs with synchronverters may investigate different relay characteristics and modes of operation of ADNs, and unbalanced loading conditions. Also, it can be extended to intercept the transient currents generated to reduce the stress on the power electronic components.

REFERENCES

[1]   Q. C. Zhong and G. Weiss, "Synchronverters: Inverters that mimic synchronous generators," *IEEE Trans. Ind. Electron.*, vol. 58, no. 4, pp. 1259–1267, 2011, doi: 10.1109/TIE.2010.2048839.

[2]   Z. Shuai, W. Huang, C. Shen, J. Ge, and Z. J. Shen, "Characteristics and Restraining Method of Fast Transient Inrush Fault Currents in Synchronverters," *IEEE Trans. Ind. Electron.*, vol. 64, no. 9, pp. 7487–7497, 2017, doi: 10.1109/TIE.2017.2652362.

[3]   S. Horowitz and A. Phadke, *Power Systems Relaying*. 2014.

[4]   A. Zahedi, "A review of drivers, benefits, and challenges in integrating renewable energy sources into electricity grid," *Renew. Sustain. Energy Rev.*, vol. 15, no. 9, pp. 4775–4779, 2011, doi: 10.1016/j.rser.2011.07.074.

[5]   CIGRE Working Group C6.11, "Development and operation of active distribution networks," *Cigre*, 2011. .

[6]   A. D. Paquette, M. J. Reno, R. G. Harley, and D. M. Divan, "Sharing transient loads : Causes of unequal transient load sharing in islanded microgrid operation," *IEEE Ind. Appl. Mag.*, 2014, doi: 10.1109/MIAS.2013.2288408.

[7]   P. L. Nguyen, Q. C. Zhong, F. Blaabjerg, and J. M. Guerrero, "Synchronverter-based operation of STATCOM to mimic synchronous condensers," *Proc. 2012 7th IEEE Conf. Ind. Electron. Appl. ICIEA 2012*, no. 2, pp. 942–947, 2012, doi: 10.1109/ICIEA.2012.6360859.

[8]   Q. C. Zhong, Z. Ma, W. L. Ming, and G. C. Konstantopoulos, "Grid-friendly wind power systems based on the synchronverter technology," *Energy Convers.*

Manag., vol. 89, pp. 719–726, 2015, doi: 10.1016/j.enconman.2014.10.027.

[9]   Q. C. Zhong, P. L. Nguyen, Z. Ma, and W. Sheng, "Self-synchronized synchronverters: Inverters without a dedicated synchronization unit," *IEEE Trans. Power Electron.*, vol. 29, no. 2, pp. 617–630, 2014, doi: 10.1109/TPEL.2013.2258684.

[10]   G. Ganev, K. Hinov, and N. Karadzhov, "Fault Current Limiters -Principles and Application," *ResearchGate*, pp. 2–8, 2012.

[11]   M. S. Alam, M. A. Y. Abido, and I. El-Amin, "Fault current limiters in power systems: A comprehensive review," *Energies*, vol. 11, no. 5, 2018, doi: 10.3390/en11051025.

[12]   M. Noe, R. Heller, W. H. Fietz, W. Goldacker, and T. Schneider, "HTS applications," in *Proceedings - Workshop on Accelerator Magnet Superconductors, Design and Optimization, WAMSDO 2008*, 2009.

[13]   Y. Yao, D. Wang, D. Jiang, and Z. Wu, "Research of the coupling transformer in the new bridge-type solid state fault current limiter system," *2008 World Autom. Congr. WAC 2008*, 2008.

[14]   M. T. Hagh and M. Abapour, "Non-superconducting fault current limiters," *Eur. Trans. Electr. Power*, 2009, doi: 10.1002/etep.247.

[15]   M. T. Hagh and M. Abapour, "Nonsuperconducting fault current limiter with controlling the magnitudes of fault currents," *IEEE Trans. Power Electron.*, vol. 24, no. 3, pp. 613–619, 2009, doi: 10.1109/TPEL.2008.2004496.

[16]   M. T. Hagh, S. B. Naderi, and M. Jafari, "Application of non-superconducting fault current limiter to improve transient stability," *PECon2010 - 2010 IEEE Int.*

Conf. Power Energy, no. 1, pp. 646–650, 2010, doi: 10.1109/PECON.2010.5697660.

[17]   M. Tarafdar Hagh, M. Jafari, and S. B. Naderi, "Transient stability improvement using Non-superconducting Fault Current Limiter," *PEDSTC 2010 - 1st Power Electron. Drive Syst. Technol. Conf.*, pp. 367–370, 2010, doi: 10.1109/PEDSTC.2010.5471789.

[18]   E. M. Leung, "Superconducting Fault Current Limiters," *IEEE Power Eng. Rev.*, vol. 20, no. 8, pp. 15–18, 2000, doi: 10.1109/39.857449.

[19]   D. K. Park *et al.*, "Analysis of the operational characteristics of a resistive SFCL by using the YBCO coated conductor," *IEEE Trans. Appl. Supercond.*, vol. 17, no. 2, pp. 1851–1854, 2007, doi: 10.1109/TASC.2007.897757.

[20]   M. R. Osorio, J. A. Lorenzo, P. Toimil, G. Ferro, J. A. Veira, and F. Vidal, "Inductive superconducting fault current limiters with Y123 thin-film washers versus Bi2223 bulk rings as secondaries," *IEEE Trans. Appl. Supercond.*, vol. 16, no. 3, pp. 1937–1942, 2006, doi: 10.1109/TASC.2006.874960.

[21]   B. W. Lee *et al.*, "Design and experiments of novel hybrid type superconducting fault current limiters," *IEEE Trans. Appl. Supercond.*, vol. 18, no. 2, pp. 624–627, 2008, doi: 10.1109/TASC.2008.920785.

[22]   X. Wang, Y. W. Li, S. Member, and F. Blaabjerg, "Virtual-Impedance-Based Control for Voltage-Source and Current-Source Converters," vol. 30, no. 12, pp. 7019–7037, 2015.

[23]   F. Salha, F. Colas, and X. Guillaud, "Virtual resistance principle for the overcurrent protection of PWM voltage source inverter," *IEEE PES Innov. Smart*

Grid Technol. Conf. Eur. ISGT Eur., pp. 1–6, 2010, doi: 10.1109/ISGTEUROPE.2010.5638965.

[24]   J. He and Y. W. Li, "Analysis, design, and implementation of virtual impedance for power electronics interfaced distributed generation," *IEEE Trans. Ind. Appl.*, vol. 47, no. 6, pp. 2525–2538, 2011, doi: 10.1109/TIA.2011.2168592.

[25]   S. Hu, X. Lin, Y. Kang, and X. Zou, "An improved low-voltage ride-through control strategy of doubly fed induction generator during grid faults," *IEEE Trans. Power Electron.*, vol. 26, no. 12, pp. 3653–3665, 2011, doi: 10.1109/TPEL.2011.2161776.

[26]   A. D. Paquette and D. M. Divan, "Virtual Impedance Current Limiting for Inverters in Microgrids With Synchronous Generators," *IEEE Trans. Ind. Appl.*, vol. 51, no. 2, pp. 1630–1638, 2015, doi: 10.1109/TIA.2014.2345877.

[27]   X. Lu, J. Wang, J. M. Guerrero, and D. Zhao, "Virtual-impedance-based fault current limiters for inverter dominated AC microgrids," *IEEE Trans. Smart Grid*, vol. 9, no. 3, pp. 1599–1612, 2018, doi: 10.1109/TSG.2016.2594811.

[28]   T. Younis, M. Ismeil, E. K. Hussain, and M. Orabi, "Single-phase self-synchronized synchronverter with current-limiting capability," *2016 18th Int. Middle-East Power Syst. Conf. MEPCON 2016 - Proc.*, pp. 848–853, 2017, doi: 10.1109/MEPCON.2016.7836994.

[29]   T. Younis, M. Ismeil, E. K. Hussain, and M. Orabi, "Improved single-phase self-synchronised synchronverter with enhanced dynamics and current limitation capability," *IET Power Electron.*, vol. 12, no. 2, pp. 337–344, 2019, doi: 10.1049/iet-pel.2018.5582.

[30] J. Roldán-Pérez, A. Rodríguez-Cabero, and M. Prodanovic, "Parallel current-controlled synchronverters for voltage and frequency regulation in weak grids," *J. Eng.*, vol. 2019, no. 17, pp. 3516–3520, 2019, doi: 10.1049/joe.2018.8218.

[31] H. H. Zeineldin, E. F. El-Saadany, and M. M. A. Salama, "Protective relay coordination for micro-grid operation using particle swarm optimization," *LESCOPE'06 2006 Large Eng. Syst. Conf. Power Eng. - Conf. Proc.*, pp. 152–157, 2006, doi: 10.1109/LESCPE.2006.280379.

[32] M. M. Mansour, S. F. Mekhamer, and N. E. S. El-Kharbawe, "A modified particle swarm optimizer for the coordination of directional overcurrent relays," *IEEE Trans. Power Deliv.*, vol. 22, no. 3, pp. 1400–1410, 2007, doi: 10.1109/TPWRD.2007.899259.

[33] F. Razavi, H. A. Abyaneh, M. Al-Dabbagh, R. Mohammadi, and H. Torkaman, "A new comprehensive genetic algorithm method for optimal overcurrent relays coordination," *Electr. Power Syst. Res.*, vol. 78, no. 4, pp. 713–720, 2008, doi: 10.1016/j.epsr.2007.05.013.

[34] P. P. Bedekar, S. R. Bhide, and V. S. Kale, "Optimum coordination of overcurrent relays in distribution system using dual simplex method," *2009 2nd Int. Conf. Emerg. Trends Eng. Technol. ICETET 2009*, pp. 555–559, 2009, doi: 10.1109/ICETET.2009.164.

[35] R. Thangaraj, M. Pant, and K. Deep, "Optimal coordination of over-current relays using modified differential evolution algorithms," *Eng. Appl. Artif. Intell.*, vol. 23, no. 5, pp. 820–829, 2010, doi: 10.1016/j.engappai.2010.01.024.

[36] M. Barzegari, S. M. T. Bathaee, and M. Alizadeh, "Optimal coordination of

directional overcurrent relays using harmony search algorithm," *2010 9th Conf. Environ. Electr. Eng. EEEIC 2010*, no. 7, pp. 321–324, 2010, doi: 10.1109/EEEIC.2010.5489935.

[37] V. Rashtchi, J. Gholinezhad, and P. Farhang, "Optimal coordination of overcurrent relays using Honey Bee Algorithm," *2010 Int. Congr. Ultra Mod. Telecommun. Control Syst. Work. ICUMT 2010*, pp. 401–405, 2010, doi: 10.1109/ICUMT.2010.5676606.

[38] P. P. Bedekar and S. R. Bhide, "Optimum coordination of directional overcurrent relays using the hybrid GA-NLP approach," *IEEE Trans. Power Deliv.*, vol. 26, no. 1, pp. 109–119, 2011, doi: 10.1109/TPWRD.2010.2080289.

[39] M. Singh, B. K. Panigrahi, A. R. Abhyankar, and S. Das, "Optimal coordination of directional over-current relays using informative differential evolution algorithm," *J. Comput. Sci.*, vol. 5, no. 2, pp. 269–276, 2014, doi: 10.1016/j.jocs.2013.05.010.

[40] F. A. Albasri, A. R. Alroomi, and J. H. Talaq, "Optimal Coordination of Directional Overcurrent Relays Using Biogeography-Based Optimization Algorithms," *IEEE Trans. Power Deliv.*, vol. 30, no. 4, pp. 1810–1820, 2015, doi: 10.1109/TPWRD.2015.2406114.

[41] V. A. Papaspiliotopoulos, G. N. Korres, and N. G. Maratos, "A Novel Quadratically Constrained Quadratic Programming Method for Optimal Coordination of Directional Overcurrent Relays," *IEEE Trans. Power Deliv.*, vol. 32, no. 1, pp. 3–10, 2017, doi: 10.1109/TPWRD.2015.2455015.

[42] W. El-Khattam and T. S. Sidhu, "Restoration of directional overcurrent relay coordination in distributed generation systems utilizing fault current limiter," *IEEE*

Trans. Power Deliv., vol. 23, no. 2, pp. 576–585, 2008, doi: 10.1109/TPWRD.2008.915778.

[43] A. S. Noghabi, J. Sadeh, and H. R. Mashhadi, "Considering different network topologies in optimal overcurrent relay coordination using a hybrid GA," *IEEE Trans. Power Deliv.*, vol. 24, no. 4, pp. 1857–1863, 2009, doi: 10.1109/TPWRD.2009.2029057.

[44] W. K. A. Najy, H. H. Zeineldin, and W. L. Woon, "Optimal protection coordination for microgrids with grid-connected and islanded capability," *IEEE Trans. Ind. Electron.*, vol. 60, no. 4, pp. 1668–1677, 2013, doi: 10.1109/TIE.2012.2192893.

[45] K. A. Saleh, M. S. El Moursi, and H. H. Zeineldin, "A new protection scheme considering fault ride through requirements for transmission level interconnected wind parks," *IEEE Trans. Ind. Informatics*, vol. 11, no. 6, pp. 1324–1333, 2015, doi: 10.1109/TII.2015.2479583.

[46] K. A. Saleh, H. H. Zeineldin, A. Al-Hinai, and E. F. El-Saadany, "Optimal Coordination of Directional Overcurrent Relays Using a New Time-Current-Voltage Characteristic," *IEEE Trans. Power Deliv.*, vol. 30, no. 2, pp. 537–544, 2015, doi: 10.1109/TPWRD.2014.2341666.

[47] H. H. Zeineldin, H. M. Sharaf, D. K. Ibrahim, and E. E. D. A. El-Zahab, "Optimal protection coordination for meshed distribution systems with DG using dual setting directional over-current relays," *IEEE Trans. Smart Grid*, vol. 6, no. 1, pp. 115–123, 2015, doi: 10.1109/TSG.2014.2357813.

[48] E. Dehghanpour, H. Kazemi Karegar, R. Kheirollahi, and T. Soleymani, "Optimal

coordination of directional overcurrent relays in microgrids by using cuckoo-linear optimization algorithm and fault current limiter," *IEEE Trans. Smart Grid*, vol. 9, no. 2, pp. 1365–1375, 2018, doi: 10.1109/TSG.2016.2587725.

[49]   A. G. T. K. Abdel-Galil, A. E. B. Abu-Elanien, E. F. El-Saadany and and H. H. M. Z. Y. A.-R. I. Mohamed, M. M. A. Salama, "Protection coordination planning with distributed generation," *Canmet Energy Technol. Centre, 2007-149/2007-09-14*, pp. 98–107, 2007.

[50]   A. H. Beg and M. Z. Islam, "Advantages and limitations of genetic algorithms for clustering records," *Proc. 2016 IEEE 11th Conf. Ind. Electron. Appl. ICIEA 2016*, pp. 2478–2483, 2016, doi: 10.1109/ICIEA.2016.7604009.

[51]   L. He, Z. Shuai, X. Zhang, X. Liu, Z. Li, and Z. J. Shen, "Transient Characteristics of Synchronverters Subjected to Asymmetric Faults," *IEEE Trans. Power Deliv.*, vol. 34, no. 3, pp. 1171–1183, 2019, doi: 10.1109/TPWRD.2019.2906766.

[52]   Univ. Washington, Power Systems Test Case Archive, Seattle, WA, "IEEE 30 bus system." [Online]. Available: http://www.ee.washington.edu/research/%0Apstca/.

VITA AUCTORIS

NAME:	Saad Pola
PLACE OF BIRTH:	Baghdad, Iraq
YEAR OF BIRTH:	1988
EDUCATION:	Al-Mutmayzeen High school, Baghdad, Iraq, 2006
	University of Technology, B.Sc., Baghdad, Iraq, 2010
	University of Windsor, HCP., Windsor, ON, 2018